Electronic and magnetic structure of 3*d*-transition-metal point defects in silicon calculated from first principles

F. Beeler* and O. K. Andersen
Max-Planck-Institut für Festkörperforschung, Postfach 80 06 65, D-7000 Stuttgart-80, Federal Republic of Germany

M. Scheffler†
Physikalisch-Technische Bundesanstalt, Bundesalle 100, D-3300 Braunschweig, Federal Republic of Germany
(Received 11 October 1988; revised manuscript received 15 May 1989)

We describe spin-unrestricted self-consistent linear muffin-tin-orbital (LMTO) Green-function calculations for Sc, Ti, V, Cr, Mn, Fe, Co, Ni, and Cu transition-metal impurities in crystalline silicon. Both defect sites of tetrahedral symmetry are considered. All possible charge states with their spin multiplicities, magnetization densities, and energy levels are discussed and explained with a simple physical picture. The early transition-metal interstitial and late transition-metal substitutional 3*d* ions are found to have low spin. This is in conflict with the generally accepted crystal-field model of Ludwig and Woodbury, but not with available experimental data. For the interstitial 3*d* ions, the calculated deep donor and acceptor levels reproduce all experimentally observed transitions. For substitutional 3*d* ions, a large number of predictions is offered to be tested by future experimental studies.

I. INTRODUCTION

Investigations of transition-metal (TM) impurities in semiconductors have received much attention in the last few years. This interest is due to purely scientific as well as technological reasons.

It is well known that the various ionized states of free TM atoms are spread over a range of more than 10 eV. However, a TM *impurity* in a covalent crystal can have a sequence of donor and acceptor levels (corresponding to different charge states) within the narrow band gap (order of 1 eV).[1–6] Thus the Coulomb repulsion energies of the free ions will have to be reduced in the solid by 1 or 2 orders of magnitude. For this to occur, a significant hybridization between impurity *d* and host *s-p* valence states is necessary, which leads to a delocalization of the impurity *d*-like orbitals and a screening of the electron-electron repulsion (due to a microscopic dielectric constant).

The *technological* relevance is based on the fact that the electronic properties of semiconductors are profoundly modified by the presence of TM impurities. Having several deep levels in the gap, these impurities mediate between valence and conduction bands and are thus efficient centers for recombination of electrons and holes.[7,8] It is therefore often the TM content which limits the lifetime of excess carriers in semiconductor devices. Very long lifetimes are demanded in electro-optical devices and contamination with 3*d*-TM defects needs often be kept at a minimum; whereas Cu contamination of 10^{16} cm^{-3} has almost no effect, merely a concentration of 10^{14} cm^{-3} Ti or V may halve the efficiency of silicon solar cells.[8,9] In fast-switching devices short carrier lifetimes are needed and may be achieved by doping of silicon with transition- or noble-metal impurities.[4,10]

Qualitative understanding of the electronic properties of single TM point defects in silicon is based on the pioneering work of Ludwig and Woodbury (LW).[1] They developed a very successful model (see Sec. II A) to interpret and analyze the electron-paramagnetic-resonance (EPR) spectra at various interstitial and substitutional 3*d*-TM ions in silicon (see Fig. 1). Up to now, the LW model has been consistent with all EPR-identified TM impurities on both T_d sites in silicon. Therefore this model is generally accepted and, as a consequence it has often been also applied to those 3*d*-TM ions where no EPR data exist (e.g., Ti^0, V^+, Ti^-, V^0, and V^-).

The aim of our theoretical study is to give a microscopic justification of the LW model and a discussion of its validity range. In order to get a fundamental and comprehensive understanding of the electronic and magnetic properties of TM impurities, we performed *spin-*

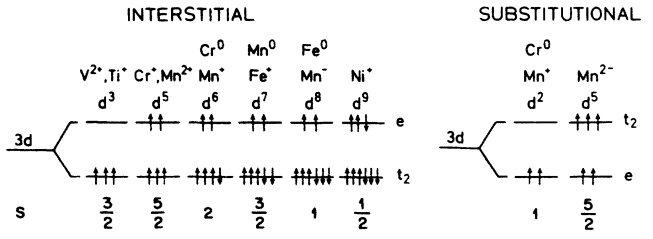

FIG. 1. 3*d* transition-metal ions which have been observed by EPR in silicon at the interstitial T_d site and the substitutional T_d site (Refs. 1 and 11). For each EPR-identified 3*d* ion the model of Ludwig and Woodbury (Ref. 1) is consistent with the known experimental data. *S* represents total electron spin.

unrestricted ab initio linear muffin-tin-orbital (LMTO) Green-function calculations (see Sec. III) of the energetically lowest spin configurations for the tetrahedral interstitial and substitutional site in silicon. The calculated total-energy differences between *high-spin* and *low-spin* configurations in the ground state were used to decide whether the basic assumption of a *Hund's-rule* occupation of the defect-induced e and t_2 states (i.e., *high-spin* ground state) in the LW model is verified. Our theory predicts *low-spin* ground states and thus a *breakdown* of Hund's rule for the *early* transition-metal interstitials Ti^0, V^+, Ti^-, V^0, and V^-, and the *late* transition-metal substitutionals Fe^0, Co^+, Ni^{2+}, Co^0, Ni^+, Co^-, Ni^0, and Cu^+. This is in conflict with the model of LW, but not with existing experimental data.

For each element of the 3*d*-TM series from Sc to Cu all possible charge states with their spin multiplicities and magnetization (or spin) densities in the ground-state configuration as well as the corresponding transition energies (i.e., donor and acceptor levels) have been calculated. Our ground-state results are in agreement with all EPR data of 3*d* ions in silicon (see Fig. 1), except for interstitial Cr: We attribute the low-spin ground states calculated for Cr^0 and Cr^+ to the local-spin-density and atomic-sphere approximations, to the gap correction, and particularly to the neglect of a breathing distortion of the impurity neighbors (*magnetic-pressure* effect; see Sec. IV B 2).

The calculated deep donor and acceptor levels for tetrahedral interstitial 3*d* ions reproduce for the first time all experimentally observed transitions. Only the double-donor level (+/2+) for Cr obtained by us is not found experimentally. This failure is consistent with the above-mentioned problem. For interstitial Co, Ni, and Cu, where no unambiguous experimental level positions are available, our calculation predicts a single-donor and a single-acceptor level for Co, but no energy level in the gap and thus no electrical activity for Ni and Cu. For V and Ti our theory predicts a *low-spin* ground state which is strongly supported by the good agreement between calculated and experimentally determined level positions: The experimental finding of a characteristic jump in the trend of the single-donor level (0/+) between interstitial V and Cr is reproduced by our calculation and is due to the switch from *low spin* to *high spin* between V and Cr.

II. EXPERIMENTAL AND THEORETICAL SITUATION

In the following we summarize the existing theoretical and experimental knowledge about 3*d* impurities in silicon that is important for the later discussion of our results. First, we present the model of Ludwig and Woodbury. In Sec. II B, a brief summary and discussion of EPR and deep-level transient-spectroscopy (DLTS) data will be given, and in Sec. II C we discuss results of previous theoretical investigations.

A. Model of Ludwig and Woodbury

The 3*d*-TM group consisting of the elements Sc, Ti, V, Cr, Mn, Fe, Co, Ni, and Cu has the atomic configuration $[Ar]3d^{n-m}4s^m$, where the number of valence electrons n goes from 3 to 11 and m equals 2, except for Cr and Cu, where it is 1.

Concerning the electronic and magnetic properties of TM atom existing as point defects in silicon, Ludwig and Woodbury gave a qualitative interpretation more than 20 years ago.[1] Based on their pioneering EPR studies, they developed the following model.

The atomic 4*s* electrons will—after incorporation of a 3*d*-TM ion into silicon at the tetrahedral (T_d point-group) interstitial or substitutional site—be promoted to the 3*d*-like orbitals: a 3*d* ion with n valence electrons is in a d^n configuration if it is T_d interstitial, and in a d^{n-4} configuration if it is T_d substitutional. In the case of substitutional ions, four of the n valence electrons are supposed to be involved in substituting the four Si electrons removed from the valence band (together with the removed Si atom) and, therefore, only $n-4$ electrons are in localized 3*d*-like states.

By incorporation of a TM ion at one of the two T_d sites in silicon, the atomic 3*d* orbital is split into doublet e and triplet t_2 states by the tetrahedral crystal field. For T_d interstitial ions, the states of t_2 symmetry are energetically lower than the states of e symmetry, whereas for substitutional ions the level ordering is reversed, i.e., the e states lie below the t_2 states.

A further assumption in the LW model is that for both the substitutional and interstitial TM ions in the ground-state configuration the t_2 and e states are populated according to *Hund's rule*, i.e., the ground states have *high spin* as in an atom where no crystal field is present. If N_e is the number of d electrons occupying the t_2 and e states, the ground state of a TM ion has total electron spin $S=N_e/2$ if $N_e \leq 5$ and $S=(10-N_e)/2$ otherwise.

The model of LW is consistent with all existing EPR data for T_d interstitial and substitutional TM ions in silicon up to now (see Fig. 1).[1,11]

B. Experimental data

Extensive experimental investigations have been performed on 3*d*-TM impurities in silicon over the last 30 years (e.g., Refs. 1, 4, and 5) using many different techniques, such as, for example, EPR, electron-nuclear double resonance (ENDOR), DLTS, and Hall effect. Here we will give a short summary of those experimental properties that allow a direct comparison with our calculated theoretical results (see Sec. III): these are, especially, EPR and DLTS data.

1. EPR

Most of the established experimental data on 3*d*-TM impurities in silicon come from the EPR study of LW carried out in the early 1960s.[1]

Figure 1 lists all 3*d*-TM ions which have been identified as isolated interstitial or substitutional impurities in silicon. With the exception of interstitial Ti^+,[11] all 3*d* ions indicated in Fig. 1 were already observed by the EPR investigations of LW. Not all elements of the 3*d*-TM series could be identified by EPR, and those which

have been identified have not been seen in all possible charge states (ions) (see Fig. 2). For example, the d^4 configuration is absent: Interstitial V has so far only been seen as a double positive charged ion and interstitial Ti as a single positive charged ion, although DLTS measurements found for both V and Ti a single-donor $(0/+)$ and -acceptor level $(-/0)$ as well as double-donor level $(+/2+)$, i.e., four different charge states for V and Ti (see Fig. 2). Further, no EPR data are available for Sc, Co, and Cu point defects.

With the exception of interstitial Ni, the defect symmetry is found to be T_d, i.e., no static, symmetry-lowering lattice distortion was found.[1,5]

The simple model of LW, discussed in Sec. II A, successfully explains the observed EPR spectra for all interstitial and substitutional $3d$-TM ions in Fig. 1.

As indicated in Fig. 1 for a $3d$-TM ion at the interstitial T_d site in silicon, the atomic $3d$ orbital is split into a doublet, e, and a triplet, t_2. At the interstitial T_d site the crystal field is assumed to arise from the incompletely screened nuclear positive charges of the four neighboring silicon nuclei as well as from the six second-nearest-neighbor silicon nuclei. As a consequence, t_2 is below e. According to the LW model, the e and t_2 states are occupied by the n valence electrons of a $3d$ ion to obey Hund's rule, i.e., it is assumed that the ground state has the highest possible spin. For example, $n=6$ for Cr^0 and Mn^+, and, according to the model of LW, interstitial Cr^0 and Mn^+ ions in silicon are in a d^6 configuration and the triplet state t_2 is occupied by four electrons and the doublet state e by two electrons, yielding a *high-spin* ground state with total electron spin $S=2$.

$3d$-TM ions clearly prefer interstitial sites in silicon, i.e., substitutional $3d$ ions could only be produced by an irradiation process out of interstitials by trapping of vacancies.[1,5]

As shown in Fig. 1, on the substitutional T_d site in silicon only three $3d$-TM ions have been observed by EPR so far.[1] According to the LW model, the t_2 states lie above the e states. Four electrons are required for bonding and the remaining $n-4$ valence electrons of the $3d$ ion populate the e and t_2 states according to Hund's rule. As a consequence, for example, Cr^0 and Mn^+ ions at the substitutional T_d site in silicon are in a d^2 configuration, and the doublet state e is doubly occupied, whereas the triplet state t_2 is empty, yielding total electron spin $S=1$.

Because the LW model is consistent with all EPR data available up to now (Fig. 1), it is generally accepted and has often been applied also to such $3d$ ions where no EPR data are available, i.e., the model was assumed to be valid for all $3d$-TM ions in silicon. However, we will show that several aspects of the crystal-field and Hund's-rule assumptions need to be modified.

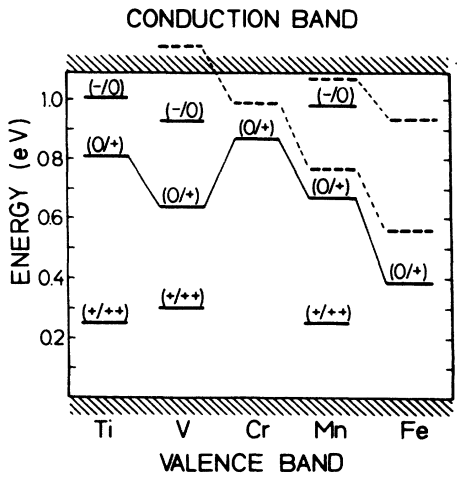

FIG. 2. Experimental energy levels of interstitial $3d$-transition-metal impurities in silicon (solid lines) (Refs. 2, 4, 5, 12, and 13) in comparison with the results of $X\alpha$ cluster calculations (Ref. 17) (dashed lines).

2. *DLTS*

The measured electrical data for TM impurities in silicon, as reviewed recently,[4,5] have to be treated with some care because often a reliably established defect configuration (point defect, pair or complex) is missing. The energy levels of interstitial $3d$-TM defects in silicon[2,4,5,12,13] which are well established are summarized in Fig. 2. In the case of interstitial Fe, Mn, and Cr for each level, the electronic defect configuration of the corresponding charge states are given by EPR analysis and the LW model. For example, for the single-donor level $(0/+)$ of Fe both the neutral and single positive charge states are identified by EPR, as can be seen in Fig. 1. However, for the energy levels of V and Ti, EPR data are available only in the case of the double positive charge state of V and the single positive charge state of Ti.

No established experimental energy-level data are available for $3d$-TM ions at the substitutional site in silicon. The single-donor level for Mn is an exception: DLTS measurements in combination with EPR analysis by Czaputa *et al.*[14] show for Mn a single-donor level $(0/+)$ at 0.38 eV above the valence-band edge.

C. Previous theoretical investigations

Most of the existing *ab initio* electron-structure calculations for TM impurities in silicon have been based on a cluster approach in which the host crystal together with the impurity atom are approximated by a finite cluster.[15–17] The dangling orbitals of the atoms at the cluster surface are often saturated by hydrogen atoms. Unfortunately, as demonstrated by DeLeo *et al.*,[17] defect calculations based on the cluster approach are hampered by considerable uncertainties due to the *size* and *termination* of the cluster.

In order to overcome these shortcomings of the cluster approach, theoretical investigations based on a self-consistent Green-function technique have been performed recently.[18–20] This treatment may be viewed as a cluster calculation where the *correct boundary conditions* are taken into account. Thus this method takes advantage of the periodicity of the host crystal as well as the localization of the defect-induced perturbation of the

effective potential. It has been demonstrated to be very efficient and powerful.

In the following a short summary of theoretical results of both methods—cluster approach and Green-function technique—will be given.

1. Cluster approach

The first electronic-structure theories for TM impurities in semiconductors were based on the cluster approach. Cartling[15] and Hemstreet[16] performed calculations of the electronic properties associated with simple *substitutional* 3*d*-TM point defects in silicon by the self-consistent scattered-wave $X\alpha$ method.[21,22] They used an $X\mathrm{Si}_4\mathrm{H}_{12}$ cluster in which the 3*d* impurity atom X was surrounded by four silicon atoms and the remaining part of the silicon crystal was simulated by 12 hydrogen atoms.

Self-consistent scattered-wave $X\alpha$ calculations of the electronic structure and energy levels of *interstitial* 3*d*-TM impurities have been carried out by DeLeo, Watkins, and Fowler using an $X\mathrm{Si}_{10}\mathrm{H}_{16}$ cluster with a 3*d*-TM element X centered at the high-symmetry (T_d) interstitial position.[17] In order to investigate the uncertainty due to the cluster termination, the hydrogen atoms have been placed at two different positions, i.e., at two different Si—H bond lengths: Si-H distance equal to the normal crystalline Si-Si distance (cluster *A*) and Si-H distance reduced by 25% (cluster *B*). The resulting spin-restricted single-particle-state energies in the region of the band gap are shown in Fig. 3 for clusters *A* and *B*. The defect-induced states are labeled t_2 and e. As shown in Fig. 3, the results depend rather strongly on the cluster termination, i.e., the Si—H bond length; for cluster *B* the crystal-field splitting between e and t_2 is much larger and the defect states are found[17] to be significantly more localized on the impurity compared with cluster *A*. Another interesting point of view is the size of the band gap: Cluster *A* has a gap of 0.84 eV, which is smaller by about a factor of 5 than in the case of cluster *B*. Inclusion of spin, i.e., a spin-unrestricted calculation for 3*d* impurities at the interstitial T_d site in silicon, which was only possible for cluster *B*, confirmed all assumptions of the LW model: All valence electrons of the impurity are in the 3*d*-derived states, which are split into a doublet e and a lower-lying triplet t_2. Hund's rule is fulfilled because the spin splitting of the e and t_2 states was calculated to be larger than the crystal-field splitting between e and t_2.

As shown in Fig. 2, the energy levels, calculated for cluster *A* including many-electron effects approximately according to the Hemstreet-Dimmock scheme,[23] reproduce the increasing trend of the single-donor level (0/+) between Fe and Cr, but clearly fail to describe the jump from Cr to V. Furthermore, the neutral and single negative charge states of interstitial V are predicted to be unstable. For interstitial iron the cluster model predicts an acceptor level deep in the gap that is not found experimentally.[5,24]

2. Green-function method

The Green-function method has been successfully applied to the study of a series of *sp*-bonded point defects in silicon.[25–29] However, for 3*d*-transition-metal impurities in silicon *ab initio spin-unrestricted* Green-function calculations have been performed only recently by

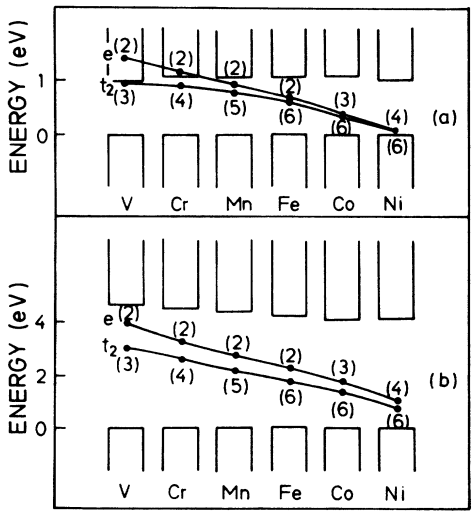

FIG. 3. Spin-restricted $X\alpha$ cluster results of the single-particle e and t_2 states induced by neutral interstitial transition-metal impurities at the center of two different $\mathrm{Si}_{10}\mathrm{H}_{16}$ clusters as calculated by DeLeo *et al.* (Ref. 17): (a) The Si-H distances are equal to the crystalline Si-Si distance (cluster *A*), and (b) 75% of the crystalline Si-Si distance (cluster *B*). Numbers in parentheses given the occupancy of the defect-induced states.

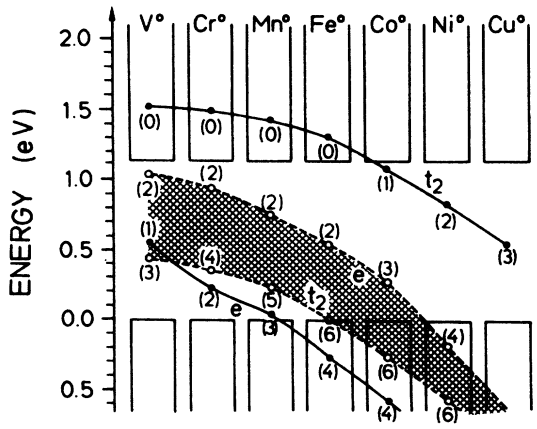

FIG. 4. Single-particle e and t_2 states induced by neutral substitutional (solid circles) and interstitial (open circles) transition-metal point defects in silicon as calculated by Lindefelt and Zunger using a local pseudopotential Green-function method (Ref. 18). Numbers in parentheses indicate occupations of the states. the crystal-field splitting for interstitial impurities is denoted by the cross-hatched area.

Katayama-Yoshida and Zunger and by us (see Sec. IV).[19,20,30]

This section will briefly discuss *spin-restricted* Green-function applications on 3*d* point defects in silicon by Zunger and Lindefelt.[18] They used local pseudopotentials and $\alpha=1$ in the exchange-correlation potential, but no spherical approximation to the potential. As shown in Fig. 4, the crystal-field splitting between the doublet e and triplet t_2 states is much larger compared with cluster calculations discussed in Sec. II C 1. It is not clear if this difference originates from the muffin-tin and cluster approximations of DeLeo *et al.*[17] or from the $\alpha=1$ approximation in the exchange-correlation potential of Zunger and Lindefelt.[18] For a comparison with experimental properties such as total electron spin or energy-level positions in the gap, *spin polarization* has to be included, i.e., a *spin-unrestricted* Green-function treatment of transition-metal impurities is needed (see below).

III. THEORY

Our calculations of deep-level defect properties reported in this paper (Sec. IV) are performed using the self-consistent Green-function technique, which is based on the linear muffin-tin-orbital (LMTO) method in the atomic-sphere approximation (ASA). The basic concept of this method for general applications to defects in crystals is given in Ref. 31. In this section we shall comment on those features of the method which are important for studies of deep impurities in semiconductor crystals such as silicons.

Within the Green-function method the impurity electronic-structure problem separates into two parts: First, after having solved the band-structure problem for the infinite crystal self-consistently, the Green function G^0 of the perfect crystal is calculated. Secondly, for reasons of convenience, to solve Dyson's equation for the defect problem, G^0 is transformed to a related Green function g^0 and then the Green function g for the crystal with the impurity is calculated by self-consistently solving Dyson's equation $g=g^0-g^0\Delta P g$ with the perturbation ΔP due to the impurity. Afterwards, g is transformed back to G.

A. Calculation of the Green function G^0 of the perfect crystal

1. Band-structure problem

In the LMTO-ASA method the solid is divided into spheres in such a way that a close-packed structure is obtained. Recognizing the relatively open diamond structure of silicon, we divide the Si crystal into space-filling spheres which are centered at all Si *and* interstitial sites. The basis set consists of s, p, and d orbitals in all spheres. In the ASA the crystal potential is spherically averaged within each sphere. For perfect crystals this approach has been shown to yield accurate charge densities, band structures, and total energies.[32] The resulting atomic-sphere potential for a crystal divided into spheres located at sites $\mathbf{R}$ with radii s_R may be written

$$V(\mathbf{r})=\sum_R \Theta(r_R/s_R)v_R(r_R)\ , \tag{3.1}$$

where the local coordinate are $\mathbf{r}_R=\mathbf{r}-\mathbf{R}$ and $\Theta(r_R/s_R)$ is a step function of unity inside a sphere of radius s_R and zero outside. The potential v_R in the sphere at site $\mathbf{R}$ is

$$v_R(r)=\mu_{xc}(n_R(r))+2\int_{\Omega_R} d^3r'\frac{n_R(r')}{|\mathbf{r}-\mathbf{r}'|}-\frac{2Z_R}{r}+\sum_{R'\neq R}\frac{2q_{R'}}{|\mathbf{R}-\mathbf{R}'|}\ . \tag{3.2}$$

We use Rydberg atomic units. The first term is the exchange-correlation potential in the Hohenberg-Kohn-Sham local-density approximation[33] (LDA), and $n_R=n_{v;R}+n_{c;R}$ is the density of the valence and core electrons. The valence-electron density $n_{v;R}$ is obtained from self-consistent band-structure calculations, and the core-electron density $n_{c;R}$ is taken from a free-atom calculation, that is, we use the frozen-core approximation. The second term is the electrostatic potential from the total electron density n_R, where the integration range Ω_R is the sphere of radius s_R at $\mathbf{R}$. The third term in Eq. (3.2) is the electrostatic potential of the nucleus and the last term is the electrostatic Madelung potential from the net charges $q_{R'}$ of all other spheres,

$$q_R=-Z_R+\int_{\Omega_R} d^3r\, n_R(r)\ , \tag{3.3}$$

where Z_R is the atomic number. The Schrödinger differential equation for the spherically symmetric potential $v_R(r)$ and an arbitrary energy E is satisfied by the partial wave

$$\phi_{RL}(E,\mathbf{r}_R)=\phi_{Rl}(E,r_R)Y_L(\hat{r}_R)\ , \tag{3.4}$$

where Y_L is a real spherical harmonic, L is a collection angular-momentum index ($\equiv\{l,m\}$), and ϕ_{Rl} is the solution of the radial Schrödinger equation for $r_R\leq s_R$. In the region between the spheres, the atomic-sphere (AS) potential (3.1) is defined to be equal to the single-particle energy E; that is, the kinetic energy $E-V(\mathbf{r})$ vanishes. Therefore it is convenient to continue the partial wave for $r_R\geq s_R$ with a tail function of zero kinetic energy outside its sphere, i.e., it is a solution of the Laplace equation. The requirement that the partial wave is continuously differentiable leads to

$$\phi_{Rl}(E,r_R)=\phi_{Rl}(E,s_R)\left[\frac{D_{Rl}(E)+l+1}{2l+1}\left(\frac{r_R}{s_R}\right)^l+\frac{l-D_{Rl}(E)}{2l+1}\left(\frac{r_R}{s_R}\right)^{-l-1}\right] \tag{3.5}$$

for $r_R\geq s_R$. In (3.5), $D_{Rl}(E)$ is the logarithmic derivative of the radial wave function, i.e.,

$$D_{Rl}(E)=\left[\frac{\partial\ln\phi(E,r_R)}{\partial\ln r}\right]_{r_R=s_R}\ . \tag{3.6}$$

In order to build a wave function at the energy E for the entire system, we construct from the partial waves the so-called muffin-tin orbitals (MTO's) $\chi_{Rl}(E,\mathbf{r}_R)$ by subtracting from $\phi_{Rl}(E,\mathbf{r}_R)$ the part which diverges at infinity as r^l. Therefore, the radial part of the MTO's which are our basis functions is

$$\chi_{Rl}(E,r_R)=\phi_{Rl}(E,s_R)\times\begin{cases}\dfrac{\phi_{Rl}(E,r_R)}{\phi_{Rl}(E,s_R)}-\dfrac{D_{Rl}(E)+l+1}{2l+1}\left[\dfrac{r_R}{s_R}\right]^l, & r_R\le s_R\\ \dfrac{l-D_{Rl}(E)}{2l+1}\left[\dfrac{r_R}{s_R}\right]^{-l-1}, & r_R\ge s_R\ .\end{cases}\tag{3.7}$$

The MTO is continuous and differentiable in all space and it is a solution of the Laplace equation outside its sphere, but it is no solution of the Schrödinger equation inside its sphere [because of the r^l term in (3.7) for the case $r_R\le s$]. The spheres are located on a lattice, i.e.,

$$\mathbf{R}=\mathbf{T}+\mathbf{U}\ ,\tag{3.8}$$

where $\mathbf{T}$ are the lattice translations and $\mathbf{U}$ the sites in the primitive cell. For the unperturbed crystal the MTO's only depend on $\mathbf{U}$. To construct a wave function for the entire system, we may now place a linear combination of MTO's at each site $\mathbf{U}$ in the primitive cell,

$$\psi(E,\mathbf{k},\mathbf{r})=\sum_{U,L}\chi_{UL}(E,\mathbf{r}_U)B_{UL}(\mathbf{k})\ ,\tag{3.9}$$

and ask whether we can determine the coefficients B such that the wave function $\psi(E,\mathbf{r})$ is a solution of Schrödinger's equation at energy E. The condition is that inside any sphere the sum of the MTO tails coming from all other sites must cancel the r^l terms from the MTO's located at that site [see Eq. (3.7)]. This leads to the following secular equations,

$$\sum_{U,L}[P_{Ul}(E)\delta_{U'U}\delta_{L'L}-S_{U'L',UL}(\mathbf{k})]\times[\dot P_{Ul}(E)]^{-1/2}B_{UL}(\mathbf{k})=0\ ,\tag{3.10}$$

for all U' and L', where $P(E)$ is the potential function, $\dot P(E)$ is its energy derivative, and $S(\mathbf{k})$ are the structure constants in the Bloch representation. The structure constant S are independent of the lattice constant, the potential, the sphere radii, and the energy. The potential function $P(E)$ is related to the logarithmic derivative of the radial wave function (3.6) through

$$P_{Ul}(E)=2(2l+1)\frac{D_{Ul}(E)+l+1}{D_{Ul}(E)-1}\ .\tag{3.11}$$

The wave function (3.9) is normalized to 1 in the primitive cell, i.e., it is

$$\sum_{U,L}|B_{UL}(\mathbf{k})|^2=1\ .\tag{3.12}$$

The logarithmic derivative function $D(E)$ [see Eq. (3.6)] for a given partial wave is a cotangentlike function with a branch for each value of the principal quantum number, and the potential function $P(E)$ is uniquely related to $D(E)$. It is convenient to parametrize the potential function (3.11) in the form

$$P_{Ul}(E)\approx\tilde P(E)=\frac{\Gamma_{Ul}}{V_{Ul}-E}+Q_{Ul}\ ,\tag{3.13}$$

where V, Γ, and Q are so-called potential parameters. The parametrization $\tilde P(E)$ is correct to second order in $E-E_\nu$, where E_ν is an arbitrary energy at which the potential function $P(E)$ is expanded. Substituting $P(E)$ in the secular equations (3.10) by $\tilde P(E)$, (3.10) is transformed into an *eigenvalue* equation,

$$\sum_{U,L}[H_{UL,U'L'}(\mathbf{k})-E\delta_{U'U}\delta_{L'L}]B_{UL}=0\ ,\tag{3.14}$$

where H is the Hamiltonian

$$H_{UL,U'L'}(\mathbf{k})=V_{Ul}\delta_{U'U}\delta_{L'L}+(\Gamma_{Ul})^{1/2}\{[Q-S(\mathbf{k})]^{-1}\}_{UL,U'L'}(\Gamma_{U'l'})^{1/2}\ .\tag{3.15}$$

The eigenvalues $E_j(\mathbf{k})$ of H equal the one-electron energies obtained from the secular equations (3.10) to second order in $E-E_\nu$. The projected density of states is

$$N_{U'L',(U+T)L}(E)=\frac{1}{V_{\rm BZ}}\sum_j\int d^3k\ e^{i\mathbf{k}\cdot\mathbf{T}}B^*_{U'L',j}(\mathbf{k})B_{UL,j}(\mathbf{k})\delta(E-E_j(\mathbf{k}))\ ,\tag{3.16}$$

where $V_{\rm BZ}$ is the Brillouin-zone volume. The spherically symmetric valence-electron density in the sphere located at $\mathbf{R}=\mathbf{U}+\mathbf{T}$ is related (3.15) through

$$n_{v;U}(r_U)=\frac{1}{4\pi}\sum_L\int dE\,[\phi_{Ul}(E,r_U)]^2N_{UL,UL}(E)\ .\tag{3.17}$$

The radial wave function $\phi_{Ul}(E,r_U)$ in (3.17) is approximated by the first two terms of the Taylor expansion,

$$\phi_{Ul}(E,r_U)=\phi_{Ul}(E_\nu,r_U)+(E-E_\nu)\dot\phi_{Ul}(E_\nu,r_U)+o(E-E_\nu)^2\ .\tag{3.18}$$

The band-structure problem is solved, i.e., the self-consistent crystal potential $v_U(r_U)$ for the sites $\mathbf{U}$ in the primitive cell is obtained by the following iterative procedure: For a given start potential $v_U^{(1)}(r_U)$, the Hamiltonian matrices (3.15) are diagonalized, and with the relations (3.16) and (3.17) the valence-electron density $n_{v;U}^{(1)}(r_U)$ and from that the corresponding potential $\bar v_U^{(1)}(r_U)$ are calculated using relation (3.2). The potential for the nth iteration is constructed from a superposition of $v_U^{(n-1)}(r_U)$ and $\bar v_U^{(n-1)}(r_U)$ with a mixing factor f ($f\le 0.1$),

$$v_U^{(n)}(r_U)=(1-f)v_U^{(n-1)}(r_U)+f\bar{v}_U^{(n-1)}(r_U) . \quad (3.19)$$

2. *Green-function G^0 of the perfect crystal*

The Green function of a perfect crystal with lattice sites $\mathbf{R}=\mathbf{T}+\mathbf{U}$, i.e., for a system of eigenvalue equations (3.14), is defined by

$$\sum_{R,L}(Z\delta_{R'R}\delta_{L'L}-H^0_{R'L',RL})G^0_{RL,R''L''}=\delta_{R'R''}\delta_{L'L''} , \quad (3.20)$$

where $Z=E+iE'$ (E,E' real, $E'\neq 0$) is a point in the complex energy plane, and H^0 is the Hamilton matrix (3.15) of the unperturbed crystal. The imaginary part of the Green function $G^0(Z)$ with $E'\to 0$ is proportional to the projected density of states of the perfect crystal,

$$\lim_{E'\to 0}\mathrm{Im}G^0_{R'L',RL}(Z)=\pi N^0_{R'L',RL}(E) , \quad (3.21)$$

and the full Green function $G^0(Z)$ is given by

$$G^0_{R'L',RL}(Z)=\int_{E_b}^{E_t}dE\frac{N^0_{R'L',RL}(E)}{Z-E} , \quad (3.22)$$

where E_b is the bottom of the lowest-energy band and E_t the top of the highest-energy band.

In order to calculate defect properties (see Sec. III B), the Green function $G^0(Z)$ is calculated for a set of energy points Z along two contours in the lower half of the complex energy plane as shown in Fig. 5, denoted γ_1 and γ_2. The rectangular path γ_1 starts on the real axis below the lower valence-band edge and ends on the real axis at the top of the valence band, whereas path γ_2 starts on the real axis above the upper valence-band edge and ends on the real axis below the conduction band. Paths γ_1 and γ_2 are needed to calculate the impurity properties associated with the defect-induced states within the valence-band and gap regions, respectively.

The valence-electron density (3.17) of the perfect crystal may be calculated by a complex energy integration along the path γ_1 as follows,

$$n_{v;U}(r_U)=\frac{1}{4\pi^2}\sum_L\int_{\gamma_1}dZ[\phi_{Ul}(Z,r_U)]^2\,\mathrm{Im}G^0_{UL,UL}(Z) , \quad (3.23)$$

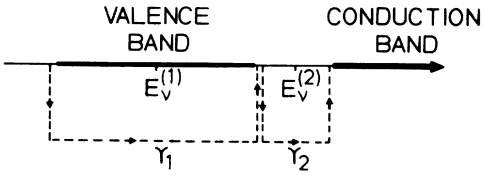

FIG. 5. Charge density of the perturbed crystal calculated using two integration paths in the complex energy plane: γ_1 for the defect-induced states in the valence band and γ_2 for the bound states in the gap. The potential function $P(E)$ is parametrized for γ_1 around an energy $E_v^{(1)}$ centered in the valence band and for γ_2 around $E_v^{(2)}$ in the center of the band gap.

where the radial wave function $\phi_{Ul}(Z,r_U)$ in (3.23) is defined by relation (3.18) with the real energy E substituted by the complex energy Z.

B. Calculation of the Green function G of the perturbed crystal

In order to solve Dyson's equation for the defect problem, we use the Green function $g^0(Z)$, which is defined by

$$\sum_{R,L}[\tilde{P}^0_{Rl}(Z)\delta_{R'R}\delta_{L'L}-S_{R'L',RL}]g^0_{RL,R''L''}=\delta_{R'R''}\delta_{L'L''} . \quad (3.24)$$

The relation between the Green function $g^0(Z)$ and $G^0(Z)$ is

$$g^0_{RL,R'L'}(Z)=-\frac{Z-V^0_{RL}}{\Gamma^0_{Rl}}\delta_{R'R}\delta_{L'L}+\frac{Z-V^0_{Rl}}{(\Gamma^0_{Rl})^{1/2}}G^0_{RL,R'L'}(Z)\frac{Z-V^0_{R'l'}}{(\Gamma^0_{R'l'})^{1/2}} . \quad (3.25)$$

Neglecting lattice distortions, the Green function $g(Z)$ for the crystal with the impurity is obtained by solving the Dyson equations

$$g_{R'L',RL}(Z)=g^0_{R'L'RL}(Z)-\sum_{R'',L''}g^0_{R'L',R'',L''}(Z)\Delta P_{R''L''}\times(Z)g_{R''L'',RL}(Z) , \quad (3.26)$$

where the perturbation $\Delta P(Z)$ due to the defect only concerns the potential functions and is limited to few diagonal elements corresponding to the impurity site and near-neighbor sites,

$$\Delta P_{RL}(Z)=[P_{Rl}(Z)-\tilde{P}^0_{RL}(Z)] . \quad (3.27)$$

The reason we switch from G^0 to g^0 is the following: Solving the Dyson equation for G leads to the perturbation $\Delta H=H-H^0$, which is, in contrast to ΔP, not diagonal in $\mathbf{R}$ and L. The size of the matrices in (3.26) is determined by the range of the perturbation ΔP. The major advantage of the Green-function method arises from the fact that the defect perturbation ΔP is large only in a small region of space, i.e., ΔP is localized. Assuming that there are N perturbed sites in total with s, p, and d orbitals on each site (i.e., $l_{\max}=2$), the matrices in Dyson's equation (3.26) have the dimension $M=N(l_{\max}+1)^2=9N$. In our calculations, the perturbation ΔP was included inside nine atomic spheres (i.e., $N=9$) centered at the impurity site, the four nearest Si sites and the four nearest interstitial sites.

It is well known that the density-functional-theory–local-density-approximation (DFT-LDA) band gap in Si is about half of the experimental value. In order to compare the calculated donor and acceptor energies with experimental data, the LDA band gap of Si was increased to the experimental value. This was done by a rigid shift of the conduction-band density of states by $\Delta=0.6$ eV, i.e., using the scissor operator, S_{sc} by Baraff

and Schlüter,[27] before calculating $G^0(Z)$ and $g^0(Z)$. However, the corresponding potential function $\tilde{P}^0_{Rl}(Z)$ is not modified. The application of the scissor operator could lead to a total energy of the perturbed system which is, compared to the LDA total energy, too high by roughly $\Delta E = N\Delta$, where N is the number of occupied conduction-band–derived states. This scissor effect is reduced within the LMTO Green-function formalism for transition-metal ions in silicon. In the orthogonal MTO representation, the scissor operator of the perturbed system $\langle \chi_{Rl}|\hat{S}_{sc}|\chi R'l'\rangle$ is related to the scissor operator of the perfect system $\langle \chi^0_{Rl}|\hat{S}_{sc}|\chi^0_{R'l'}\rangle$ by

$$\langle \chi_{Rl}|\hat{S}_{sc}|\chi_{R'l'}\rangle \approx (\Gamma_{Rl}/\Gamma^0_{Rl})^{1/2}\langle \chi^0_{Rl}|\hat{S}_{sc}|\chi^0_{R'l'}\rangle \times(\Gamma_{R'l'}/\Gamma^0_{R'l'})^{1/2} , \quad (3.28)$$

where $\Gamma^0_{Rl}, \chi^0_{Rl}$ and Γ_{Rl}, χ_{Rl} are the potential parameters and MTO's of the pure host and perturbed system, respectively. For a TM d orbital Γ is from 3.6 (Ti) to 11 (Cu) times smaller than Γ^0 for the substituted Si, and from 4.5 (Ti) to 16 (Cu) times smaller than Γ^0 for the interstitial-sphere d orbital.

For the perturbed crystal the space-group symmetry of the pure crystal is reduced to a point group of rotations $\hat{\mathcal{R}}$. In order to keep the matrices a manageable size, we transform from the site and real spherical harmonic representation (3.4) to the symmetry representation given by the following functions,[22]

$$f^{\alpha}_{\kappa\mu,RL}(\mathbf{r}) = \sum_{\mathcal{R}} \Gamma^{\alpha}_{\kappa\mu}(\mathcal{R})\hat{\mathcal{R}}\phi_{RL}(\mathbf{r}_R)\Theta(r_R/s_R) , \quad (3.29)$$

where $\Gamma^{\alpha}_{\kappa\mu}(\mathcal{R})$ are the matrices of the αth irreducible representation of the point group. The functions f are linearly dependent, in general. Thus we have only to keep a smaller number linearly independent functions and, from them, an orthonormal basis set is formed.

For reasons of efficiency and accuracy, the Dyson equations (3.26) are solved for a path in the complex energy plane because here the structure in the Green function is smoothed out.[34] For a start potential V^{in}_1 for the perturbed crystal, (3.26) is solved for a set of energy points Z along the contour γ_1 for the defect-induced states in the valence band and along the contour γ_2 for the bound states in the gap region (see Fig. 5). The Green function $g^{0(j)}$ for the pure crystal is calculated for an energy E_v in the center of the contour γ_j. After transforming from the symmetry representation back into the site and angular-momentum representations, the spherically symmetrized charge density of the perturbed region is obtained by

$$n_{v;R}(r) = (4\pi)^{-1}\sum_L \sum_{j=1}^{2} b_j \int_{\gamma_j} dZ[\phi^{(j)}_{Rl}(Z,r_R)]^2 \times N^{(j)}_{RL,RL}(Z) , \quad (3.30)$$

where

$$N^{(j)}_{RL,RL}(Z) = \frac{1}{\pi}\dot{P}^{(j)}_{Rl}(Z)\text{Img}^{(j)}_{RL,RL}(Z) \quad (3.31)$$

and

$$\phi^{(j)}_{Rl}(Z,r_R) := \phi_{Rl}(E^{(j)}_v,r_R) + (Z-E^{(j)}_v)\dot{\phi}_{Rl}(E^{(j)}_v,r_R) + \tfrac{1}{2}(Z-E^{(j)}_v)^2\ddot{\phi}_{Rl}(E^{(j)}_v,r_R) . \quad (3.32)$$

The occupation number $b_j = 1$ for the defect-induced states in the valence band ($j=1$) and depends on the charge state of the defect for the bound state in the gap region ($0 \le b_2 \le 1$). From (3.30) and relation (3.2), V^{out}_1 is calculated and, in analogy to (3.19), the start potential for the second iteration is built from a superposition of V^{in}_1 and V^{out}_1.

The magnetization is, within the local-spin-density-functional approximation,[33] described by the difference between the exchange-correlation potentials for the spin-up and spin-down electrons,

$$v^{\uparrow}_{\text{xc}} - v^{\downarrow}_{\text{xc}} = \tfrac{2}{3}\vartheta(n(\mathbf{r}))\mu_x(n(\mathbf{r}))\frac{m(\mathbf{r})}{n(\mathbf{r})} , \quad (3.33)$$

where μ_x is the exchange part of the exchange-correlation potential[33] and

$$n(\mathbf{r}) = n^{\uparrow}(\mathbf{r}) + n^{\downarrow}(\mathbf{r}) , \quad (3.34)$$

$$m(\mathbf{r}) = n^{\uparrow}(\mathbf{r}) - n^{\downarrow}(\mathbf{r}) \quad (3.35)$$

are the total electron density and spin density, respectively. The magnetization is reduced with decreasing electron density $n(\mathbf{r})$ by the function $\vartheta(n(\mathbf{r}))$. The spin splitting Δ_x of a transition-metal-induced single-particle state ϕ in the gap region is, in first-order perturbation theory, given by the Stoner expression

$$\Delta^{\text{Stoner}}_x = 2S\left[\frac{m_0}{m}\right]\alpha^2 I_0 , \quad (3.36)$$

where I_0 is the Stoner parameter and $m = 2S$ the integral of the spin density in all space, and

$$\alpha^2(\phi) = \int_I d^3r\,|\phi|^2 , \quad (3.37)$$

$$m_0 = \int_I d^3r\, m(\mathbf{r}) \quad (3.38)$$

are the localization factor of ϕ and the integral of the spin density in the impurity sphere I, respectively.

Total-energy differences between different possible charge (ion) states, i.e., donor and acceptor energies, are calculated by the transition-state concept of Slater.[22(b)] For all charge states considered, the net induced charge inside the perturbation region (impurity, four nearest Si sites, and four nearest interstitial sites) was found to differ by less than 0.05 electron from the asymptotic value q/ϵ, where q is the charge of the TM ion and ϵ the Si dielectric constant. For charged impurity states the contribution to the total energy of the long-range Coulomb potential, $-2q(\epsilon r)^{-1}$ Ry, which is not included within the perturbation region considered in the Green-function treatment, is taken to be $-q(0.1\text{ eV})$.[35]

IV. RESULTS

A. Spin-restricted calculations

For the discussion to follow it is useful to consider, at first, *spin-restricted* electronic-structure calculations of

$3d$-TM ions in silicon, i.e., to neglect the effect of spin polarization. This allows one to compare our results with previous spin-restricted theoretical investigations.[17,18] In Sec. IV B we will show that the effects due to spin polarization can be significant and, for an analysis of experimental data, they have to be included.

1. *Substitutional site*

Here we take Mn as an example. The changes in the density of states (DOS) induced by a neutral substitutional Mn atom in silicon are shown in Fig. 7. For reasons of relevance, only states of A_1 (s-like at the impurity), E (d-like at the impurity), and T_2 (p- and d-like at the impurity) symmetries are displayed. In the following—after having analyzed the different contributions to the induced DOS of Mn—we will discuss the trend of the defect-induced states of A_1, E, and T_2 symmetry through the $3d$ series from V to Cu. For each symmetry, the results will be discussed and explained in terms of a simple physical picture.

(a) induced DOS of A_1 symmetry. The a_1-induced DOS associated with neutral $3d$-TM impurities can be understood by a comparison with the vacancy-induced a_1 states (see Fig. 6). As shown in Fig. 7, for $Si:Mn^0_{sub}$ the states of A_1 symmetry are very similar to the induced a_1 states of the unrelaxed silicon vacancy. Integration of the induced a_1 states over the valence band gives zero contribution, i.e., no extra state of A_1 symmetry is induced in the valence band. Qualitative similar results for the A_1 symmetry are obtained for the other $3d$ impurities, except for one modification: As one goes through the $3d$ series from V to Cu, the $2a_1$ resonance in the valence band moves to lower energies, hybridizing more strongly with the valence band and therefore getting broader (see Fig. 8). A further valence-band resonance $1a_1$ is found at $E_v - 7.8$ eV through the whole $3d$ series. This sharp resonance, which is pinned at the position of a cusp of the silicon density of states, is a typical result for all substitutional defects in silicon.

The defect-induced states of A_1 symmetry can be understood qualitatively in terms of a simple physical picture which is illustrated in Fig. 9: First, we remove a Si atom from the perfect Si crystal, producing an undistorted Si vacancy (where the impurity will be inserted). As can be seen in Fig. 6 from the calculated induced DOS of A_1 symmetry associated with an unrelaxed vacancy in silicon, there are two dominant a_1 resonances in the

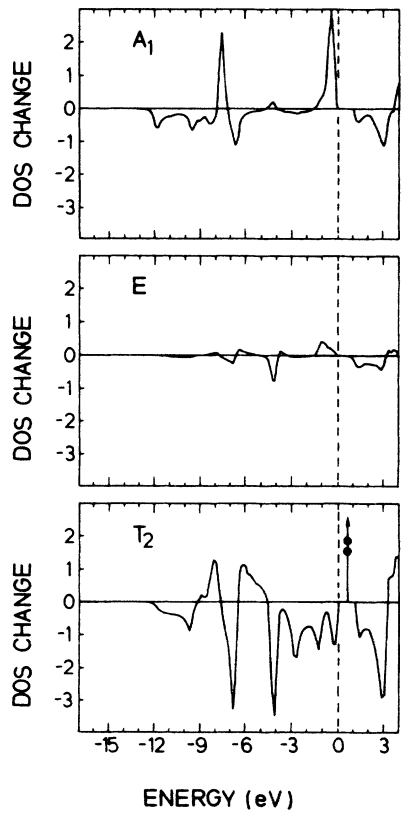

FIG. 6. Changes in the DOS of A_1, E, and T_2 symmetries induced by a neutral (unrelaxed) vacancy in silicon. The energy zero is the top of the valence band.

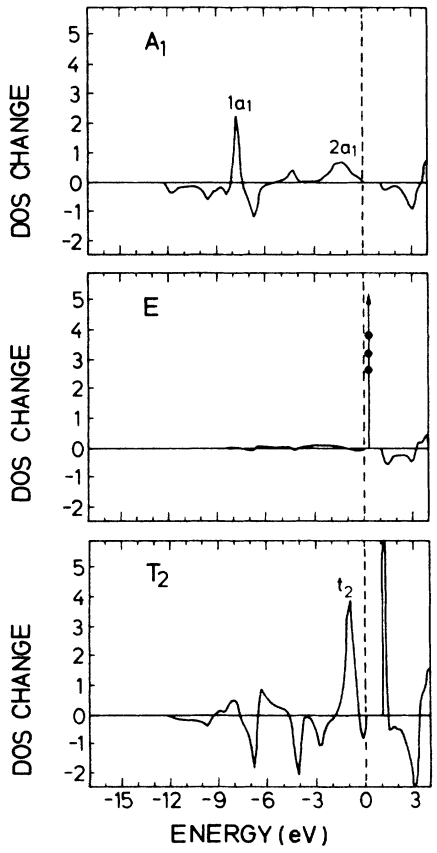

FIG. 7. Changes in the DOS of A_1, E, and T_2 symmetries induced by a substitutional neutral Mn point defect in silicon resulting from *spin-restricted* calculations. The energy zero is the top of the valence band.

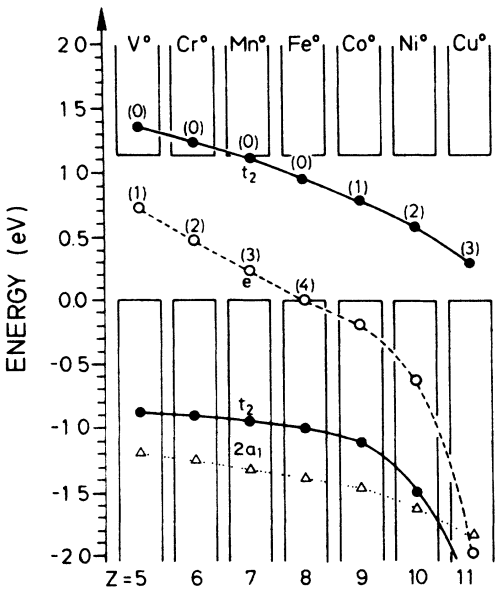

FIG. 8. Defect-induced states of neutral substitutional $3d$-transition-metal impurities in silicon (see text). The energy zero is set at the valence-band maximum. Numbers in parentheses give the occupancy of the bound states in the gap.

valence band. The first resonance just below the top of the valence band is largely built from the dangling sp^3 hybrids of the four nearest neighbors of the vacancy. The second a_1 resonance around E_v-8 eV originates from an A_1 combination of the twelve sp^3 backbonds of the four nearest vacancy neighbors.[36,37] At first, both systems in Fig. 9 (depicted in the left and right parts)—the Si vacancy and the free $3d$ atom—are assumed to be decoupled. By switching on the interaction between the two vacancy a_1 states and the $4s$ orbital of the $3d$ atom, the qualitative result in Fig. 9 (middle part) occurs. Because the $4s$-

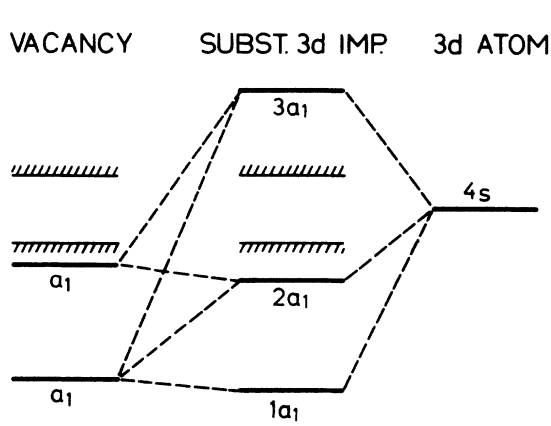

FIG. 9. Schematic description of the induced states of A_1 symmetry associated with a substitutional $3d$-transition-metal impurity in silicon (see text).

orbital energy is in the vicinity of the vacancy a_1 dangling-bond-like state, the resulting bonding orbital goes down in energy and broadens considerably. The corresponding antibonding orbital is pushed up in energy into the conduction band. In contrast, the low-lying second a_1 vacancy state interacts only weakly with the $4s$ atomic orbital. The results of our theory for the induced states of A_1 symmetry (Figs. 7 and 8) and the corresponding schematic description in Fig. 9 explain the origin of the assumption in the LW model that the atomic $4s$ electrons will—after incorporation of a $3d$ ion into silicon at the substitutional T_d site—be promoted to the $3d$-like orbitals (see Sec. II A): The antibonding $3a_1$ state in Fig. 9 lies high up in the conduction band and thus remains empty, and because of the limited energy range in Fig. 8 it is not shown there.

(b) Induced DOS of E and T_2 symmetry. As shown in Fig. 7, a neutral substitutional Mn point defect in silicon produces a bound state of E symmetry occupied by three electrons in the gap, a t_2 resonance at E_v-1 eV in the valence band, and a sharp t_2 resonance at the bottom of the conduction band. We remind the reader that Fig. 7 displays results of spin-restricted calculations. Inclusion of spin polarization gives rise to drastic changes (see Sec. IV B).

In Fig. 8 the trend of the defect-induced states of E (denoted e) and T_2 symmetry (denoted t_2) through the $3d$ series from V^0_{sub} to Cu^0_{sub} is shown.

In the case of E symmetry, Cu^0_{sub}, Ni^0_{sub}, Co^0_{sub}, and Fe^0_{sub} induce very sharp valence-band resonance states which—with decreasing atomic number—increase in energy from E_v-2 eV for Cu^0_{sub} to $E_v-0.01$ eV for Fe^0_{sub}. For these elements four new extra states are produced in the valence band. For neutral Mn, Cr, and V, instead of an e resonance there is a fourfold-degenerate localized bound state occupied by three, two, and one electron(s), respectively, increasing in energy from $E_v+0.23$ eV for Mn^0_{sub} to $E_v+0.73$ eV for V^0_{sub}.

In the case of T_2 symmetry, Cu^0_{sub}, Ni^0_{sub}, Co^0_{sub}, and Fe^0_{sub} induce bound states (see Fig. 8) in the gap which increase in energy going backwards in the $3d$ series from $E_v+0.30$ eV for Cu^0_{sub} to $E_v+0.93$ eV for Fe^0_{sub}. For Fe^0_{sub} the bound state t_2 enters the conduction band and is transformed into an empty sharp resonance state in the conduction band. Moving from Mn toward V, the resonance state t_2 smoothly increase in energy from $E_v+1.13$ eV for Mn^0_{sub} to $E_v+1.35$ eV for V^0_{sub}. Furthermore, as shown in Fig. 8, a valence-band resonance of T_2 symmetry lying systematically below the states of E symmetry is induced, which is increasing in energy backwards through the $3d$ series from $E_v-2.5$ eV for Cu^0_{sub} to $E_v-0.9$ eV for V^0_{sub}.

Figure 10 gives a schematic summary of the calculated induced DOS of E and T_2 symmetries: We begin to consider an undistorted Si vacancy and take into account only the bound state t_2 in the gap which originates from the dangling sp^3 hybrids of the four nearest vacancy neighbors. As can be seen in Fig. 6 from the calculated vacancy-induced DOS, the contribution of the states of E symmetry is small and therefore we neglect the e states in

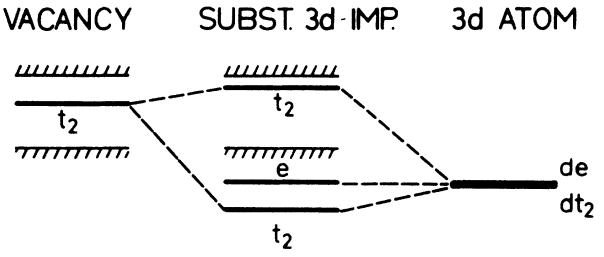

FIG. 10. Schematic description of the defect-induced states of E and T_2 symmetries associated with a substitutional $3d$-transition-metal point defect in silicon (see text).

our schematic description for the vacancy. Furthermore, we consider a free $3d$-TM ion. At first, both systems in the left and right parts of Fig. 10—the Si vacancy and the free $3d$-TM atom—are assumed to be decoupled. The middle part of Fig. 10 shows the qualitative result from switching on the interaction between the vacancy t_2 state and the atomic $3d$ orbital. Whereas the t_2 state of the vacancy interacts with the dt_2 part (xy, yz, zx) of the atomic $3d$ orbital, the de part (x^2-y^2, $3z^2-r^2$) essentially feels no interaction with the crystal states. As a consequence, the e states remain atomiclike and well localized, whereas the t_2 states become more delocalized (see Sec. IV B). The qualitative model in Fig. 10 describes the calculated results of neutral substitutional impurities Fe, Co, Ni, and Cu in silicon (see Fig. 8) because here the defect-induced e state is indeed a valence-band resonance. For V, Cr, and Mn the model can easily be modified by shifting the atomic $3d$ level to higher energies and, in turn, the resonance e moves up (as a bound state) into the gap and the bound state t_2 becomes a conduction-band resonance. From the model in Fig. 10, it follows that the t_2 valence-band resonance has *bonding* character and the t_2 bound state in the gap *antibonding* character, whereas the defect-induced e resonance in the valence band is essentially *nonbonding*. Therefore the valence-band resonance t_2 lies below the defect state e through the whole $3d$ series from Cu^0_{sub} to V^0_{sub} (see Figs. 7 and 8). The assumption in the LW model that a $3d$ ion with n valence electrons—after incorporation into silicon at the substitutional site—is in a d^{n-4} configuration is confirmed by our calculation and can be explained by the schematic description in Figs. 10 and 9: The result of the interaction between the neutral vacancy (t_2 is occupied by two electrons, see Fig. 6) and the atomic $3d$ orbital is a bondinglike valence-band resonance t_2 filled by six electrons. Thus, four of the n valence electrons of the $3d$ ion are needed to substitute for the four missing Si electrons removed from the valence band and, because the $4s$ orbital is pushed up as an empty resonance state into the conduction band, $n-4$ electrons are (except for Ni and Cu) in rather localized $3d$-like states. The further assumption in the LW model that, for a substitutional $3d$ ion, the e state is energetically lower than the t_2 state is also confirmed by our theory and explained by the simple model in Fig. 10. The decreasing splitting in energy between the valence-band resonance t_2 and the e state as well as the increasing splitting between the defect states e and t_2 (antibonding t_2) going through the $3d$ series from V to Cu can also be explained by the model in Fig. 10: Moving from V towards Cu the energy of the atomic $3d$ orbital is decreasing and therefore the interaction between the vacancy t_2 state and the $3d$ orbital of the transition-metal atom is weakened. Thus, for Ni and Cu the t_2 state in the gap is vacancy dangling-bond-like.

2. *Interstitial T_d site*

As for the substitutional site, we take Mn as an example in the following discussion of our calculated spin-restricted results for T_d interstitial $3d$-TM point defects in silicon. The total induced DOS associated with a neutral interstitial Mn atom in silicon is shown in Fig. 11. Only states of A_1 (s-like at the impurity), E (d-like at the impurity), and T_2 (p- and d-like at the impurity) symmetries are displayed.

(a) Induced DOS of A_1 symmetry. As shown in Fig. 11 a neutral interstitial Mn impurity in silicon induces an a_1 resonance just above the bottom of the conduction band as well as three valence-band resonances at $E_v-4.2$ eV, $E_v-6.8$ eV, and $E_v-11.8$ eV. Integration of the induced states of A_1 symmetry over the valence-band re-

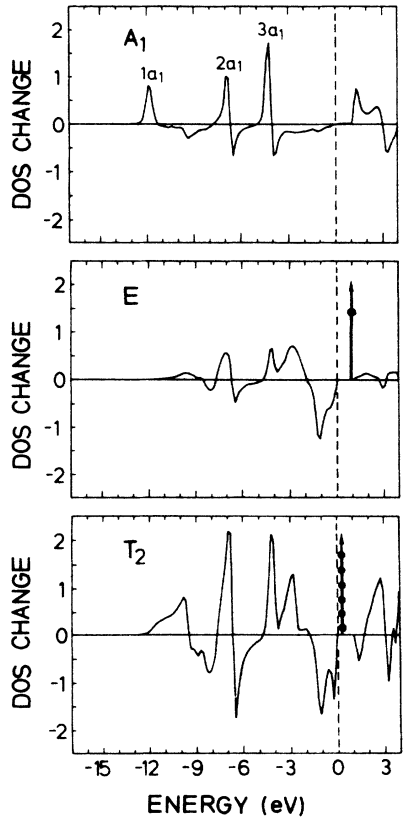

FIG. 11. Total changes in the DOS of A_1, E, and T_2 symmetries induced by an interstitial neutral Mn point defect in silicon resulting from *spin-restricted* calculations. The energy zero is at the top of the valence band.

gion gives zero contribution, i.e., no extra state of A_1 symmetry in the valence band is induced by the impurity in total. Qualitatively very similar results for the a_1 DOS are obtained for the other interstitial $3d$ impurities. Moving through the $3d$ series from neutral V to Ni, the a_1-resonance state in the conduction band becomes sharper and—as shown in Fig. 12—decreases in energy.

The calculated states of A_1 symmetry induced by an interstitial $3d$ impurity in silicon can understood qualitatively by the simple physical model illustrated in Fig. 13.

A free $3d$ atom is incorporated in a silicon crystal at the interstitial T_d site. From the calculated local density of states of the perfect Si crystal at the interstitial T_d site (see Fig. 14), we include the three valence-band resonances of A_1 symmetry as representative states in our simple model (Fig. 14, left part). By switching on the interaction between the $4s$ orbital of the $3d$ atom and the crystal states originating from the interstitial T_d site, the atomic $4s$ orbital is pushed up as a resonance state into the conduction band and the a_1-resonance states of the crystal are lowered in energy, giving rise to three valence-band resonances. As illustrated in Fig. 13, no extra state of A_1 symmetry is produced by the atomic $4s$ orbital in the valence band or the gap region. This is in agreement with the assumption in the LW model that the $4s$ electrons are promoted to $3d$-like orbitals after interstitial incorporation of a $3d$-TM ion in silicon (see Sec. II A).

(b) Induced DOS of E and T_2 symmetry. A neutral interstitial Mn impurity in silicon induces bound states of E and T_2 symmetries in the gap occupied by one and six electron(s), respectively (see Fig. 11). Figure 12 displays the trend for the neutral interstitial $3d$ series from V^0_{int} to Ni^0_{int} in the vicinity of the gap. Interstitial Cu is not included in this figure because it only exists in the single

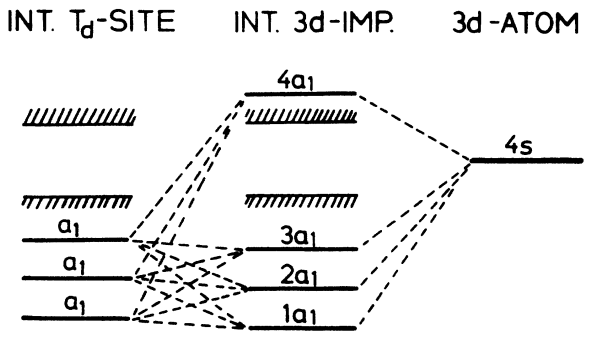

FIG. 13. Schematic description of the induced states of A_1 symmetry associated with an interstitial $3d$-transition-metal impurity in silicon.

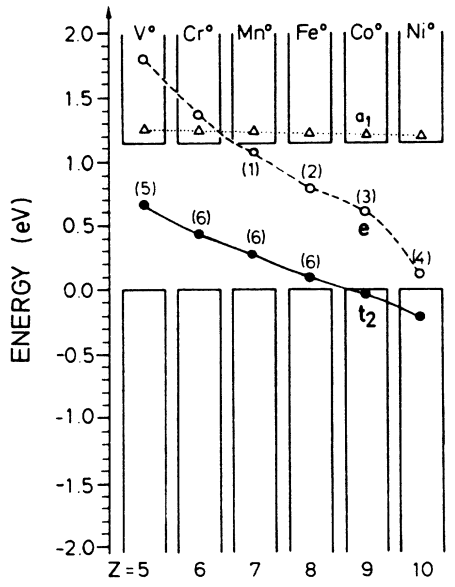

FIG. 12. Defect-induced states of neutral T_d interstitial $3d$-transition-metal impurities in silicon resulting from *spin-restricted* calculations. The energy zero is at the valence-band maximum. Numbers in parentheses give the occupancy of the bound states in the gap. Resonances inside the valence and conduction bands are assumed to be completely filled or empty, respectively.

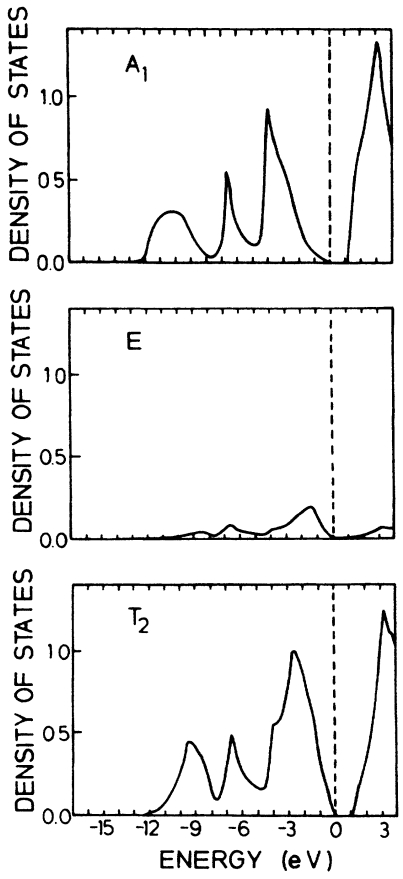

FIG. 14. Density of states of A_1, E, and T_2 symmetries of the T_d interstitial site in crystalline silicon.

positive charge state.

In the case of T_2 symmetry, Ni^0_{int} and Co^0_{int} induce sharp valence-band resonances. Between Co^0_{int} and Fe^0_{int} the t_2 resonance crosses the valence-band edge.

In the case of E symmetry, Mn^0_{int}, Fe^0_{int}, Co^0_{int}, and Ni^0_{int} cause bound gap states with decreasing energy from $E_v+1.03$ eV for Mn^0 to $E_v+0.12$ eV for Ni^0. Between Mn^0 and Cr^0 the bound state e crosses the conduction-band edge and, thus, for neutral interstitial Cr and V a conduction-band resonance e is induced.

As illustrated in Fig. 15, the results of Fig. 13 can be understood as follows: From the calculated DOS of the perfect Si crystal at the interstitial T_d site (see Fig. 11), we consider the valence-band resonance of E symmetry centered at $E_v-1.4$ eV and the two t_2-resonance states in the valence band centered at $E_v-2.4$ eV and in the conduction band at $E_v+3.2$ eV as representative states (Fig. 15, left part). The qualitative result obtained after switching on the interaction between the $3d$ orbital of the $3d$-TM atom and the crystal states of E and T_2 symmetries originating from the interstitial T_d site is given in the middle part of this figure. Because of the interaction between the dt_2 part (xy, yz, and zx) of the atomic $3d$ orbital and two t_2 crystal states, and between the de part (x^2-y^2, $3z^2-r^2$) of the $3d$ orbital and the crystal valence-band state e, the defect-induced state t_2 in the gap lies below e (Fig. 15, middle part). Therefore the level ordering t_2 *below* e for interstitial $3d$ ions in silicon comes from the fact that the Si crystal conduction band has t_2, but essentially no e, character at the T_d interstitial site. Thus the assumption in the LW model that the defect states e lie above t_2 for interstitial $3d$ impurities (Sec. II A) is confirmed by our calculations, as well as explained by the schematic description in Fig. 15. Furthermore, the decreasing crystal-field splitting between e and t_2 going through the $3d$ series from V to Ni—as shown in Fig. 12—can be understood by the model in Fig. 15: Moving from V towards Ni, the energy of the atomic $3d$ orbital decreases and, therefore, the interaction between the crystal conduction-band state t_2 and the dt_2 part of the atomic $3d$ orbitals is reduced.

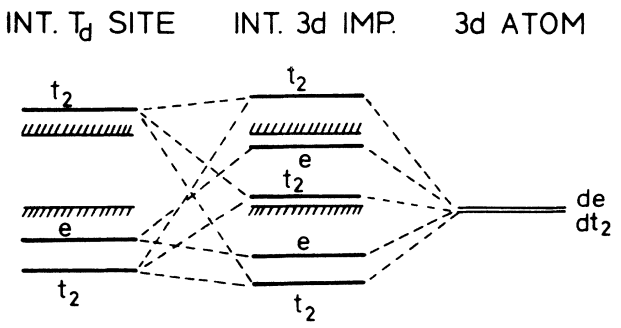

FIG. 15. Schematic description of the defect-induced states of E and T_2 symmetries associated with an interstitial $3d$-transition-metal point defect in silicon.

3. *Comparison of spin-restricted results with previous calculations*

Figure 16 displays the calculated single-particle defect-induced states e and t_2 of substitutional and T_d interstitial neutral $3d$-TM point defects in silicon. In comparison with the results of previous spin-restricted theoretical investigations[17,18] (see Sec. II C), we find the following notable features.

(i) Our calculated e-t_2 splitting for interstitial $3d$ impurities is essentially larger than that calculated in the cluster approximation by DeLeo *et al.*[17] [compare Fig. 3(a) with Fig. 16]. In *qualitative* agreement with other authors,[17,18] we find that the e-t_2 splitting increases for substitutional TM ions with increasing atomic number (i.e., from Ti to Cu). On the other hand, for interstitial TM ions the e-t_2 splitting is found to decrease with increasing atomic number.

(ii) In the calculation of Zunger and Lindefelt, the occupation numbers of the defect states e and t_2 induced by neutral interstitial $3d$ impurities are chosen (not calculated) to obey Hund's rule (see Fig. 4). Our calculated defect-induced states e and t_2 of neutron interstitial impurities lie about 0.2 eV higher in energy than those of Zunger and Lindefelt, and, as a consequence, in our theory Hund's-rule occupation (by neglect of spin polarization) is not possible for interstitial V and Cr. In the case of neutral interstitial Cr and V, spin-restricted calculations allow only a ground-state configuration with *low spin* because the induced single-particle state e appears as a conduction-band resonance and therefore cannot be occupied. For neutral substitutional $3d$ impurities,

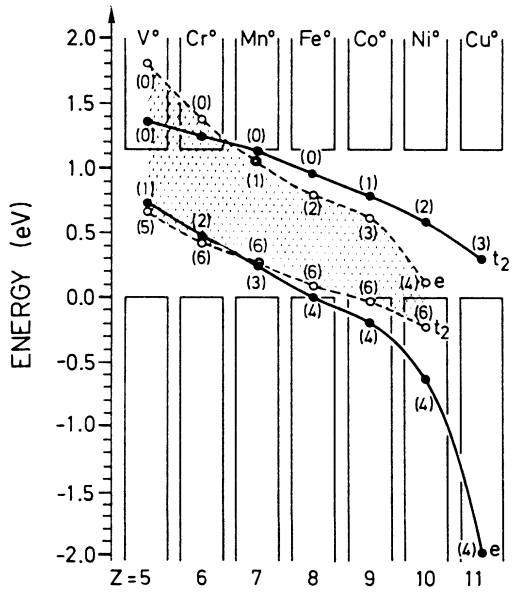

FIG. 16. Single-particle states e and t_2 induced by neutral substitutional (solid circles) and interstitial (open circles) transition-metal point defects in silicon resulting from *spin-restricted* calculations. Numbers in parentheses indicate occupations of the states. The e-t_2 splitting for interstitial impurities is denoted by the shaded area.

Hund's-rule occupation of the induced states t_2 and e could only be achieved in the case of V^0, Cr^0, and Cu^0, in agreement with the spin-restricted results of Zunger and Lindefelt (see Fig. 4).

B. Spin-unrestricted calculations

1. Substitutional site

The *spin-unrestricted* results obtained by our theory for the ground-state configuration of neutral *substitutional* 3*d*-TM impurities in silicon are shown in Fig. 17. Table I gives the calculated localization α^2 (see Sec. III) of the defect-induced states $t_2^{\uparrow}$, $t_2^{\downarrow}$, $e^{\uparrow}$, and $e^{\downarrow}$ in the band gap, the spin splitting Δ_x of the doublet state e and triplet state t_2, and the total electron spin S of the neutral *substitutional* 3*d* series Ti, V, Cr, Mn, Fe, Co, Ni, and Cu in silicon in the ground state. In Table II all calculated possible impurity charge states with the corresponding ground-state symmetries, spin multiplicities, and magnetization densities are listed. In the following we will focus on the trend of the electronic and magnetic impurity properties going through the 3*d* series.

(a) Wave-function localization, spin splitting, and spin densities. From the simple picture in Fig. 10, it follows that the impurity triple state t_2 in the gap has *antibonding* character, whereas the doublet state e is essentially *nonbonding*. Consistently, the defect-induced e states are well localized and the antibonding t_2 states are more extended (see Table I). The trend that the delocalization of the triplet state t_2 increases from Fe^0 to Cu^0 can also be explained by the schematic model in Fig. 10: With increasing atomic number the energy of the atomic 3*d* orbital is lowered and, therefore, the interaction between the dt_2 part of the atomic 3*d* orbital and the dangling-bond vacancy t_2 state is reduced. As a consequence, the antibonding t_2 impurity state gets more dangling-bond-like from Fe^0 towards Cu^0.

The trend of the calculated spin splitting $\Delta_x(t_2)$ and $\Delta_x(e)$ of the defect-induced t_2 and e states can be understood by the Stoner expression (3.36).

Going backwards through the 3*d* series from Cu^0 towards Co^0, the splitting $\Delta_x(t_2)$ between $t_2^{\uparrow}$ and $t_2^{\downarrow}$ remains of the same order of magnitude, although the total electron spin S decreases from $S=\frac{3}{2}$ for Cu^0 to $S=\frac{1}{2}$ for Co^0. This is a consequence of the localization α^2 of the $t_2^{\uparrow}$ and $t_2^{\downarrow}$ states which increases along the 3*d* series from Cu^0 to Co^0 (see Table I) and nearly compensates for the effect of the decreasing total electron spin. For Co^0 the $S=\frac{5}{2}$ configuration $e^{\uparrow}(2)e^{\downarrow}(0)t_2^{\uparrow}(3)t_2^{\downarrow}(0)$ is an excited state lying roughly 0.4 eV above the ground state.

Neglecting lattice relaxation, substitutional Fe^0 is found to be nonmagnetic: The single-particle state e

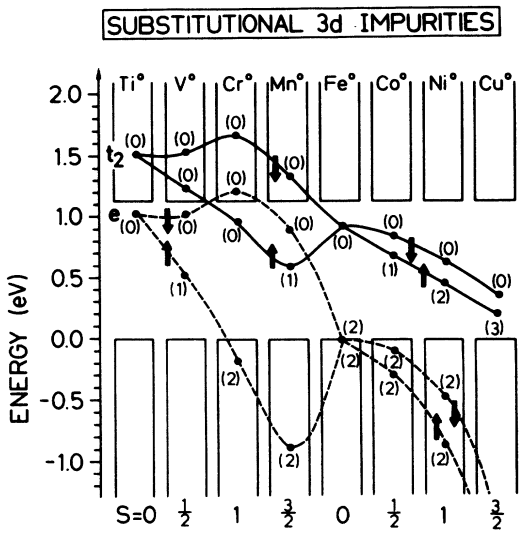

FIG. 17. Single-particle energies of the defect-induced states t_2 and e for the ground state of the neutral substitutional 3*d* impurities in silicon obtained from *spin-unrestricted* theory. A number in parentheses gives the occupancy of a localized gap state, or of a resonance in the valence or conduction band from which the total electron spin S results. Substitutional Sc only exists in the single negative charge state and is therefore not shown here.

TABLE I. Calculated localization α^2 of the defect-induced states $t_2^{\uparrow}$, $t_2^{\downarrow}$, $e^{\uparrow}$, and $e^{\downarrow}$ in the band gap, spin splitting Δ_x of the doublet state e and triplet state t_2, and total electron spin S of the neutral *substitutional* 3*d*-transition-metal point defects Ti, V, Cr, Mn, Fe, Co, Ni, and Cu in silicon in the ground state.

	$\alpha^2(t_2^{\uparrow})$	$\alpha^2(t_2^{\downarrow})$	$\alpha^2(e^{\uparrow})$	$\alpha^2(e^{\downarrow})$	$\Delta_x(e)$ (eV)	$\Delta_x(t_2)$ (eV)	S
Ti^0_{sub}					0.00	0.00	0
V^0_{sub}			0.66	0.57	0.50	0.25	$\frac{1}{2}$
Cr^0_{sub}	0.30				1.40	0.74	1
Mn^0_{sub}	0.23			0.66	1.78	0.73	$\frac{3}{2}$
Fe^0_{sub}	0.35	0.35			0.00	0.00	0
Co^0_{sub}	0.31	0.34			0.20	0.16	$\frac{1}{2}$
Ni^0_{sub}	0.24	0.28			0.37	0.19	1
Cu^0_{sub}	0.14	0.17			0.45	0.12	$\frac{3}{2}$

TABLE II. Calculated possible charge (ion) states of *substitutional* 3*d*-transition-metal impurities in silicon in the ground-state configuration d^{n-4} for $n=4,5,\ldots,11$. The different rows denote the impurity-type TM and its charge state q, the occupations of the t_2 and e states, the symmetry Γ and the spin multiplicity $2S+1$ of the many-electron ground state, the ratio m_0/m of the local magnetic moment m_0 in the impurity atomic sphere to the total magnetic moment m ($m=2S$, where S is the total electron spin), and the ratio n_0/Z between the electronic charge n_0 and the core charge Z in the impurity sphere. EPR-identified states are underlined.

SUBSTITUTIONALS

d^{n-4}	d^0			d^1	d^2			d^3		d^4				d^5			d^6			d^7		
TM^q	Sc^-	Ti^0	V^+	V^0	V^-	$\underline{Cr^0}$	$\underline{Mn^+}$	Cr^-	Mn^0	Fe^0	Co^+	Ni^{++}	Mn^-	Co^0	Ni^+	$\underline{Mn^-}$	Co^-	Ni^0	Cu^+	Co^-	Ni^-	Cu^0
t_2								↑					↑↑	↑		↑↑↑	↑↑			↑↑↑		
e				↑	↑↑			↑↑		↑↑↓↓			↑↑	↑↑↓↓		↑↑	↑↑↓↓			↑↑↓↓		
$2S+1\Gamma$		$^1A_1$		^2E		$^3A_2$			$^4T_1$		$^1A_1$		$^5T_2$		$^2T_2$	$^6A_1$		$^3T_1$			$^4A_2$	
m_0/m (%)	-	-	-	99	79	120	130	94	100	-	-	-	81	48	40	73	61	38	22	60	41	25
n_0/Z_0 (%)	65	75	81	82	83	87	89	87	89	94	93	94	90	93	94	90	94	95	95	95	95	95

is completely filled with four electrons and the t_2 state is empty. Nevertheless, the configuration $e^{\uparrow}(2)e^{\downarrow}(0)t_2^{\uparrow}(2)t_2^{\uparrow}(0)$ with total electron spin $S=2$ is higher in energy by about 0.2 eV.

Going from Fe^0 to Mn^0, the total electron spin S changes from $S=0$ to $S=\frac{3}{2}$, for the following reason: Whereas for Cu^0, Ni^0, and Co^0 the doublet states $e^{\uparrow}$ and $e^{\downarrow}$ give no direct contribution to the magnetization and spin-density, respectively, because $e^{\uparrow}$ as well as $e^{\downarrow}$ are valence-band resonances and are thus completely filled, in the case of substitutional Mn^0 only $e^{\uparrow}$ appears as a resonance (filled by two electrons) in the valence band and $e^{\downarrow}$ is an empty bound state in the gap. As will be discussed later [subsection (c)], the change in spin from $S=0$ for Fe^0 to $S=\frac{3}{2}$ for Mn^0 is caused by the change from a *low-spin* to a *high-spin* ground-state configuration. The large spin splitting $\Delta_x(e)=1.78$ eV for Mn^0_{sub} reflects the rather strong localization of e states (see Table I). As a consequence, the $t_2^{\uparrow}$ and $e^{\downarrow}$ states cross, i.e., the triplet state $t_2^{\uparrow}$ lies energetically below the doublet state $e^{\downarrow}$. Therefore in the ground-state configuration of Mn^0_{sub} the triplet $t_2^{\uparrow}$ is occupied by one electron and the doublet $e^{\downarrow}$ remains empty. In general, such a level crossing arises if the averaged spin splitting $\Delta_x(e,t_2)=[\Delta_x(e)+\Delta_x(t_2)]/2$ overcomes the crystal-field splitting between t_2 and e. As can be seen by comparing the results for substitutional Mn^0 obtained by our spin-restricted theory (see Figs. 7 and 16) and spin-unrestricted theory (see Fig. 17), the inclusion of spin polarization is particularly important here. The effect of spin polarization is not only the transformation from the configuration $e(3)t_2(0)$ to $e^{\uparrow}(2)e^{\downarrow}(1)t_2^{\uparrow}(0)t_2^{\downarrow}(0)$ with total electron spin $S=\frac{1}{2}$. As illustrated in Fig. 17, the $S=\frac{1}{2}$ configuration is not found to be the ground-state configuration of substitutional Mn^0: The internal electron transition process in which the electron in the doublet state $e^{\downarrow}$ is promoted to the triplet state $t_2^{\downarrow}$ is exothermic by 0.25 eV, and, therefore, Mn^0_{sub} has the ground-state configuration $e^{\uparrow}(2)e^{\downarrow}(0)t_2^{\uparrow}(1)t_2^{\downarrow}(0)$ with total electron spin $S=\frac{3}{2}$.

For substitutional Cr^0 the triplet state $t_2^{\uparrow}$ in the gap is empty, the doublet state $e^{\uparrow}$ lies, as in the case of Mn^0_{sub}, as a resonance in the valence band, and $e^{\downarrow}$ is an empty resonance in the conduction band. Therefore the ground state of Cr^0_{sub} has total electron spin $S=1$.

Moving from Cr^0_{sub} towards V^0_{sub}, the valence-band resonance $e^{\uparrow}$ crosses the valence-band edge and becomes a bound state in the gap that is occupied by one electron. Therefore, as follows from the Stoner expression (3.36), the spin splitting $\Delta_x(e)$ is drastically reduced for V^0_{sub} and no $e^{\downarrow}$-$t_2^{\uparrow}$ level crossing occurs as in the case of substitutional Cr^0 and Mn^0.

For neutral substitutional Ti, both defect-induced states t_2 and e are empty, and thus Ti^0_{sub} is nonmagnetic.

By fitting the Stoner expression (3.36) to our calculated spin splitting Δ_x, we obtain $I_0=0.9\pm0.1$ eV for all substitutional 3*d* ions in silicon. In Table II the ratio m_0/m between the local magnetic moment m_0 in the impurity atomic sphere and the total magnetic moment $m=2S$ (see Sec. III) is summarized for all calculated possible charge states of 3*d*-TM point defects in silicon in the ground-state configuration. For a discussion of the calculated magnetization-density results, it is meaningful to divide m_0/m into two parts: one part, $(m_0/m)_B$, which originates from defect-induced states with *unpaired* spins only, and another part, $(m_0/m)_{VB}$, which arises from the spin polarization of *completely filled* states, mostly lying in the valence band. The ratio $(m_0/m)_B$, which, in the case of 3*d* ions, is produced by the defect states e and/or t_2 with unpaired spins (not completely filled states), is

$$\left[\frac{m_0}{m}\right]_B=\frac{1}{2S}\sum_{i\in I}\mathrm{sign}(i)\alpha^2(i)n(i)\ , \tag{4.1}$$

where $n(i)$ is the occupation number of the defect state i and the summation range I is defined as

$$I=\begin{cases} e^{\uparrow},e^{\downarrow} & \text{if } n(e^{\uparrow})\neq n(e^{\downarrow}) \text{ and } n(t_2^{\uparrow})=n(t_2^{\downarrow})\ , \\ t_2^{\uparrow},t_2^{\downarrow} & \text{if } n(t_2^{\uparrow})\neq n(t_2^{\downarrow}) \text{ and } n(e^{\uparrow})=n(e^{\downarrow})\ , \\ e^{\uparrow},e^{\downarrow},t_2^{\uparrow},t_2^{\downarrow} & \text{if } n(e^{\uparrow})\neq n(e^{\downarrow}) \text{ and } n(t_2^{\uparrow})\neq n(t_2^{\downarrow})\ . \end{cases} \tag{4.2}$$

sign(i) depends only on the spin of the defect state i: It is sign(i)$=+1$ for single-particle states with spin up ($\uparrow$) and sign(i)$=-1$ with spin down ($\downarrow$). The magnetic-

moment ratio $(m_0/m)_{\mathrm{VB}}$ originating from spin polarization of *completely* filled states is

$$\left[\frac{m_0}{m}\right]_{\mathrm{VB}}=\frac{m_0}{m}-\left[\frac{m_0}{m}\right]_B . \tag{4.3}$$

For both substitutional and interstitial (see Sec. IV B 2) 3*d*-TM impurities in silicon, the magnetic-moment part, $(m_0/m)_{\mathrm{VB}}$, is, in general, very important: Whereas for substitutional Co^0 the t_2-induced magnetic-moment ratio $(m_0/m)_B=\alpha^2(t_2^{\uparrow})=0.31$ [see relation (4.1)], and thus the valence-band contribution is only $(m_0/m)_{\mathrm{VB}}=0.17$, in the case of Mn^0_{sub} the magnetic-moment part produced by the spin splitting of the valence-band states is, according to relations (4.1) and (4.3), $(m_0/m)_{\mathrm{VB}}=m_0/m-\frac{1}{3}[2\alpha^2(e^{\uparrow})+\alpha^2(t_2^{\uparrow})]=0.48$, which is nearly as large as $(m_0/m)_B=0.52$ (see Tables I and II). In the case of substitutional Cr^0 and Mn^+, the local magnetic moment m_0 in the impurity atomic sphere is even exceeding the total magnetic moment $m=2S$ ($m_0>m$ in Table II) and therefore the integration of the magnetization density $m(\mathbf{r})$ over the region outside the impurity sphere gives a negative contribution.

(b) Charge states ground-state symmetries, and spin multiplicities. All calculated charge (ion) states of substitutional 3*d* impurities in silicon in the ground-state configuration d^{n-4} for $n=4,5,\ldots,11$ are listed in Table II. For each charge state the electronic configuration, i.e., the occupations of the defect-induced states t_2 and e, are denoted, and the corresponding many-electron ground state is characterized by its spin multiplicity $(2S+1)$ and the representation Γ of the tetrahedral point group. Neglecting lattice relaxations, we find *low-spin* ground states for the substitutional 3*d* ions Fe^0, Co^+, Ni^{2+}, Co^0, Ni^+, Co^-, Ni^0, and Cu^+, which is in conflict with the generally accepted model of Ludwig and Woodbury. Unfortunately, these ions have not been identified by EPR until now. Those substitutional 3*d* ions for which EPR data exist are underlined in Table II and they have all high-spin (i.e., Hund's rule) ground states, in agreement with the LW model and with our calculated results. As listed in the last row of Table II, the ratio n_0/Z between the electronic charge n_0 and the core charge Z in the impurity sphere increases from 0.75 to 0.95 through the 3*d* series of the neutral substitutional ions and, thus, the total charge of the impurity sphere decreases from $Q=1.0$ for Ti^0 to $Q=0.5$ for Cu^0. An interesting result is that the charge in the ratio n_0/Z by changing the charge state is only 1% or less. The reason is that the charge density of an electron added or subtracted in a localized state in the gap is mainly canceled by charge rearrangements in the valence band so that local charge neutrality (within the impurity sphere) is nearly maintained.

(c) Single-particle energies and donor and acceptor levels. The calculated single-particle energies associated with neutral substitutional 3*d*-TM point defects in the ground state are shown in Fig. 17. The atomic 3*d* orbital is split into a triplet t_2 branch (solid curve in Fig. 17) and a doublet e branch (dashed curve in Fig. 17), both consisting of spin-up ($\uparrow$) and spin-down ($\downarrow$) states. As illustrated in the simple physical picture in Fig. 9, the atomic 4*s* orbital is interacting with the vacancy dangling-bond a_1-resonance state just below the upper valence-band edge and is pushed up as an empty resonance state into the conduction band and therefore not shown in Fig. 17. The spin-unrestricted results in Fig. 17 can be understood by the schematic description in Fig. 10 applied to spin-up and spin-down states. As assumed by LW, the e branch is energetically lower than the t_2 branch (see Fig. 17), which can be explained by the simple model in Fig. 10 in analogy to the spin-restricted results (Sec. IV A 1). Further, the model in Fig. 10 explains the increasing crystal-field splitting $\Delta(e,t_2)$ between the t_2 and e branches with increasing atomic number from $\Delta(e,t_2)=0.5$ eV for Ti^0 to $\Delta(e,t_2)=1.2$ eV for Ni^0. However, considering the occupation numbers of the defect states t_2 and e, respectively, the total electron spin S, the following is found: Going through the 3*d* series from substitutional Ti^0 to Cu^0, there is a characteristic jump between Mn^0 and Fe^0 interrupting the otherwise monotonous decrease of the triplet $t_2^{\uparrow}$ and doublet $e^{\uparrow}$ energy which is caused by a change from *high-spin* to *low-spin* ground states. This change from high spin to low spin between Mn^0_{sub} and Fe^0_{sub} originates from the fact that the splitting between the t_2 and e branches increases with increasing atomic number and dominates over the spin splitting in the cases of Fe, Co, Ni, and Cu. Thus for the substitutional 3*d* elements to the right of Mn, our theory indicates a *breakdown* of the LW model. Nevertheless, in the case of Fe and possibly Co the high-spin configurations are higher in energy by only few 0.1 eV and thus the neglect of lattice relaxations may be crucial.

The calculated donor and acceptor levels of substitutional 3*d* impurities in silicon that correspond to electron transitions between different possible charge states are shown in Fig. 18. For each level the related single-particle state and its occupation number before and after the ionization is indicated. For example, the single-donor level $(0/+)$ of Mn (denoted $t_2^{\uparrow}1/0$) is related to the single-particle state $t_2^{\uparrow}$ in Fig. 17 with the change in the occupation number 1/0 because it is originating from an electron transition process between Mn^0 and Mn^+ in which the electron in the triplet state $t_2^{\uparrow}$ is promoted to the conduction band. The relation between the single-donor level $(0/+)$ and the single-particle state $t_2^{\uparrow}$ is given by self-consistent transition-state calculation in which the single-particle state $t_2^{\uparrow}$ is occupied by half an electron (see Sec. III). Therefore, as a consequence of the electronic relaxation, the single-donor energy $E(0/+)=E_v+0.49$ eV of substitutional Mn is lying 0.10 eV below the single-particle energy of the $t_2^{\uparrow}$ triplet state associated with neutral substitutional Mn in Fig. 17. Consequently, the single-acceptor level $E(-/0)=E_v+0.69$ eV associated with substitutional Mn (denoted $t_2^{\uparrow}2/1$ in Fig. 18) is equal to the self-consistently calculated single-particle energy of the $t_2^{\uparrow}$ state occupied by 3/2 electrons. Thus the effective electron-electron interaction energy U, defined as the energy difference between the single-acceptor and -donor levels related to the same single-particle state, is found to be $U(t_2^{\uparrow})=0.20$ eV for substitutional Mn. The

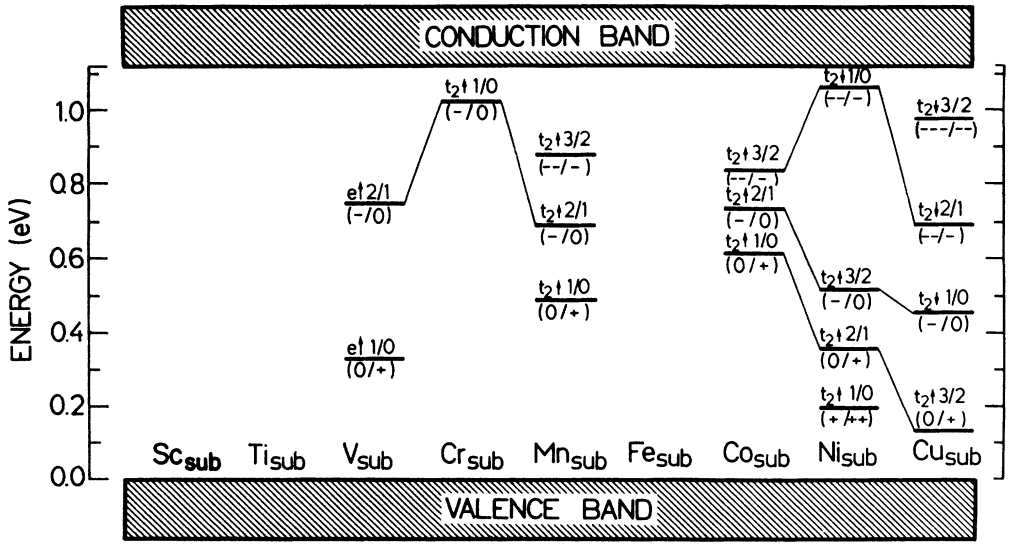

FIG. 18. Donor and acceptor levels for substitutional 3*d* impurities in silicon resulting from *spin-unrestricted* calculations. For each level the related single-particle state (see Fig. 17) and its occupation before and after the ionization is indicated.

energy levels found for substitutional Cr, Mn, Co, Ni, and Cu are all related to the triplet state $t_2^{\uparrow}$, except for the double-acceptor level $(2-/-)$ of Ni and the three acceptor levels of Cu, which are derived from $t_2^{\downarrow}$. The single-donor and -acceptor level of substitutional V are both assigned to the doublet state $e^{\uparrow}$, and, because for substitutional 3*d* ions in silicon *e* is more localized than t_2 (Table I), the corresponding effective Coulomb repulsion energy $U(e^{\uparrow})=0.42$ eV is much larger than $U(t_2^{\uparrow})$ found for Mn, Co, and Ni. However, the Coulomb repulsion energy *U* found for substitutional 3*d* impurities in silicon is 1–2 orders of magnitude smaller than the Coulomb repulsion energy of free 3*d* ions. The reason for this is the fact that the charge density of an electron added or subtracted in a bound state in the gap (which can be rather localized; see Table I) is nearly cancelled by charge rearrangements in the valence band such that the charge in the impurity sphere almost remains unchanged (see ratio n_0/Z for different charge states in Table II). This nonlinear compensation effect is the reason a substitutional 3*d*-TM impurity can have a sequence of donor and acceptor levels within the narrow band gap of silicon.

Substitutional Sc, Ti, and Fe are predicted to be electrically inactive, i.e., to have no energy level in the gap. In the case of Fe, this is a consequence of its low-spin ground-state configuration. The high-spin configuration of substitutional Fe is found to be only 0.2 eV higher in energy than the calculated low-spin ground state, and high-spin Fe is predicted to act as a single donor and a double acceptor. Thus, including lattice relaxations, the high-spin configuration may be energetically favored (*magnetic pressure* effect[32]).

For 3*d*-TM impurities at the substitutional site in silicon, there are no established experimental level positions because in most cases the defect geometry is not realiably established. The recent DLTS measurements on substitutional Mn, combined with EPR investigations by Czaputa *et al.*,[14] are an exception: They found that Mn has a single-donor level 0.39 eV above the valence-band edge and no further level below. This is in good agreement with our calculated single-donor energy of substitutional Mn (see Fig. 18).

2. *Interstitial T_d site*

The *spin-unrestricted,* defect-induced, single-particle spectrum calculated for the ground states of neutral *interstitial* 3*d*-TM impurities in silicon is shown in Fig. 19. As will be explained later, for interstitial Cr^0 the high-spin state was used. Interstitial Cu is found to exist only in the single positive charge state, and thus no results are shown in Fig. 19 for Cu. In Table III we summarize our results for the localization α^2 (see Sec. III) of the defect states $t_2^{\uparrow}$, $t_2^{\downarrow}$, $e^{\uparrow}$, and $e^{\downarrow}$ in the band gap, the spin splitting Δ_x of the doublet state *e* and triplet state t_2, and the total electron spin *S* through the neutral *interstitial* 3*d* series Ti, V, Cr, Mn, Fe, Co, Ni, and Cu in silicon in the ground-state configuration. All calculated impurity charge states found to exist with their corresponding ground-state symmetries, spin multiplicities, and magnetization densities are listed in Table IV. In the following we will focus on the trend of the electronic and magnetic impurity properties going through the 3*d* series.

(a) Wave-function localization, spin splitting, and spin densities. As illustrated in Fig. 15, the doublet state *e* and triplet state t_2 induced by interstitial 3*d* ions in silicon are, to a first approximation, *nonbonding*, and the level order t_2 below *e* originates from the fact that at the interstitial T_d site the upper part of the Si valence band has strong t_2, and some *e*, character, whereas the lower part of the conduction band has strong t_2, but essentially no *e*, character. The result obtained by our theory that

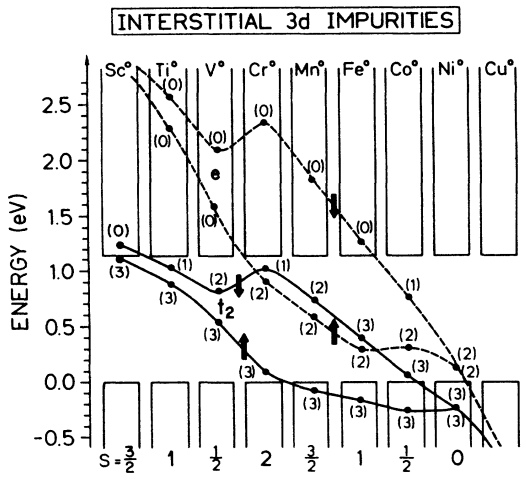

FIG. 19. Single-particle energies of the defect-induced states e and t_2 for the ground state of the neutral interstitial 3d impurities in silicon obtained from *spin-unrestricted* theory. A number in parentheses gives the occupancy of a localized gap state, or of a resonance in the valence or conduction band from which the total electron spin S results. For interstitial Cr^0 the high-spin state was used. Interstitial Cu only exists in the single positive charge state.

the localization $\alpha^2(t_2)$ for both spin-up and spin-down components of the triplet state t_2 is increasing going through the 3d series can be explained by the model in Fig. 15: With increasing atomic number, the atomic 3d orbital energy is decreasing and therefore the interaction between the dt_2 part of the atomic 3d orbital (Fig. 15, right part) and the t_2 states of the lower conduction band (Fig. 15, left part) is reduced.

Considering the results shown in Fig. 19, we first discuss the trend of the calculated spin splitting Δ_x of the defect-induced states e and t_2 going from interstitial Ni^0 to Sc^0.

For interstitial Ni^0 the bound doublet state e as well as the valence-band resonance triplet state t_2 are completely filled, resulting in $S=0$ for the total electron spin. Thus, Ni^0_{int} is nonmagnetic.

The spin polarization of interstitial Co^0 is induced by the partially filled bound state e in the gap: $e^\uparrow$ is completely filled, whereas $e^\downarrow$ is occupied by one electron. The resulting spin is $S=\frac{1}{2}$. As a consequence of the e-induced spin splitting for Co^0_{int}, the triplet state t_2 is split into a resonance $t_2^\uparrow$ in the valence band and a bound state $t_2^\downarrow$ in the gap occupied by three electrons.

The magnetization for interstitial neutral Fe originates from the doublet state e as in the case of Co^0_{int}, but the spin splitting Δ_x for Fe^0_{int} is about twice as large (see Table III). The reason is, because $e^\downarrow$ is an empty resonance in the conduction band, both electrons in the $e^\uparrow$ state contribute to the spin polarization, resulting in a total electron spin $S=1$ for interstitial Fe^0. The average spin splitting $\Delta_x(e,t_2)=[\Delta_x(t_2)+\Delta_x(e)]/2=0.75$ eV is larger than the crystal-field splitting $\Delta(e,t_2)=0.68$ eV, which results in a crossing of the $e^\uparrow$ and $t_2^\downarrow$ states (see Fig. 19), i.e., the doublet state $e^\uparrow$ lies energetically below the triplet state $t_2^\downarrow$.

In the case of interstitial Mn^0 and Cr^0, additionally to the doublet state e, the triplet state t_2 contributes to the magnetization: Whereas the $t_2^\uparrow$ state remains completely filled as in the case of Fe^0_{int}, the $t_2^\downarrow$ state is occupied by two electrons for Mn^0 and one electron for Cr^0. Going from Mn^0 to Cr^0, the crossing of the $e^\uparrow$ and $t_2^\downarrow$ states is nearly constant because the increasing spin splitting Δ_x for e and t_2 (see Table III) is almost compensated for by the increasing splitting between e and t_2 [see subsection (c)].

Moving backwards through the 3d series from Ni^0 to Cr^0, the total electron spin S is increasing in steps of $\frac{1}{2}$. However, going from Cr^0 to V^0 there is a jump in the spin from $S=2$ to $S=\frac{1}{2}$. The reason is that between Cr^0 and V^0 the bound doublet state $e^\uparrow$ (occupied by two electrons for Cr^0) is crossing the conduction-band edge (see Fig. 19), thus inducing an internal electron transition process in which the two $e^\uparrow$ electrons are transferred to the triplet state $t_2^\downarrow$. Therefore, in the case of V^0 the doublet state $e^\uparrow$ appears as an empty resonance in the conduction band, and thus the magnetization originates solely from the rather delocalized triplet state t_2 (see Table III). This has the consequence that, going from Cr^0 to V^0, the spin

TABLE III. Calculated localization α^2 of the defect-induced states $t_2^\uparrow$, $t_2^\downarrow$, $e^\uparrow$, and $e^\downarrow$ in the band gap, spin splitting Δ_x of the doublet state e and triplet state t_2, and total electron spin S of the neutral T_d *interstitial* 3d-transition-metal point defects Ti, V, Cr, Mn, Fe, Co, and Ni in silicon in the ground state. Interstitial Cu only exists in the single positive charge state.

	$\alpha^2(t_2^\uparrow)$	$\alpha^2(t_2^\downarrow)$	$\alpha^2(e^\uparrow)$	$\alpha^2(e^\downarrow)$	$\Delta_x(e)$ (eV)	$\Delta_x(t_2)$ (eV)	S
Ti^0_{int}	0.33	0.26			0.36	0.22	1
V^0_{int}	0.40	0.37			0.54	0.27	$\frac{1}{2}$
Cr^0_{int}		0.33	0.54		1.39	0.93	2
Mn^0_{int}		0.44	0.55		1.23	0.82	$\frac{3}{2}$
Fe^0_{int}		0.48	0.51		0.94	0.56	1
Co^0_{int}			0.54	0.62	0.44	0.29	$\frac{1}{2}$
Ni^0_{int}			0.52	0.52	0.00	0.00	0

TABLE IV. Calculated possible charge (ion) states of T_d *interstitial* 3*d*-transition-metal impurities in silicon in the ground-state configuration d^n for $n=2,3,\ldots,10$. The different rows denote the impurity-type TM and its charge state q, the occupations of the t_2 and e states, the symmetry Γ and the spin multiplicity $2S+1$ of the many-electron ground state, the ratio m_0/m of the local magnetic moment m_0 in the impurity atomic sphere to the total magnetic moment m ($m=2S$, where S is the total electron spin), and the ratio n_0/Z between the electronic charge n_0 and the core charge Z in the impurity sphere. EPR-identified states are underlined.

INTERSTITIALS

d^n	d^2	d^3	d^4	d^5		d^6		d^7	d^8	d^9	d^{10}
TM^q	Sc^+ Ti^{++}	Sc^0 $\underline{Ti^+}$ V^{++}	Ti^0 V^+	Cr^{++}	Ti^- V^0 Cr^+	$(\underline{Cr^+})$ Mn^{++}	V^- Cr^0	$(\underline{Cr^0})$ Mn^+	$\underline{Mn^0}$ $\underline{Fe^+}$	$\underline{Mn^-}$ $\underline{Fe^0}$ Co^+	Co^0	Co^- Ni^0 Cu^+
e	↑↑	↑↑↑	↑↑↑↓	↑	↑↑↑↓↓	↑↑	↑↑↑↓↓	↑↑	↑↑	↑↑	↑↑↑	↑↑↑↓
t_2				↑↑↑		↑↑↑		↑↑↑↓	↑↑↑↓↓	↑↑↑↓↓	↑↑↑↓↓↓	↑↑↑↓↓↓
$2S+1\Gamma$	$^3T_1$	$^4A_2$	$^3T_1$	^5E	$^2T_2$	$^6A_1$	$^1A_1$	$^5T_2$	$^4T_1$	$^3A_2$	^2E	$^1A_1$
m_0/m (%)	27 48	30 42 55	46 59	70	63 70 61	66 64	- -	70 70	81 73	99 88 73	84	- - -
n_0/Z_0 (%)	79 84	80 85 90	86 91	92	87 92 93	93 94	93 94	93 94	96 96	96 97 97	98	99 99 99

splitting Δ_x of both the e and t_2 states is drastically reduced, and thus the $e^{\uparrow}$-$t_2^{\downarrow}$ crossing which occurs for Fe^0, Mn^0, and Cr^0 is removed.

Going from V^0 to Ti^0, the spin splitting $\Delta_x(t_2)$ is reduced because of the decreasing localization α^2 of the triplet state $t_2^{\downarrow}$ from $\alpha^2(t_2^{\downarrow})=0.37$ for V^0 to $\alpha^2(t_2^{\downarrow})=0.26$ for Ti^0, which cannot be compensated for by the fact that in the case of Ti^0 one electron more is contributing to the magnetization ($S=\frac{1}{2}$ for $V^0_{\rm int}$, but $S=1$ for $Ti^0_{\rm int}$).

The calculated spin splitting Δ_x of the defect states e and t_2 can, in first-order perturbation theory, be approximated by the Stoner expression (3.36) (see Sec. III), where m_0 and m are the integrals of the magnetization density $m(\mathbf{r})$ in the impurity sphere and in all space, respectively. For all T_d interstitial 3*d* ions in silicon, it is found that $I_0\approx 0.9$ eV for the TM Stoner parameter. In Table IV the calculated magnetic-moment ratios m_0/m for all charge states found to exist for interstitial 3*d*-TM point defects in silicon are summarized. In analogy to the substitutional ions, it is meaningful to divide the magnetic-moment ratio m_0/m into a part, $(m_0/m)_B$, which originates from defect-induced states with *unpaired* spins [see relation (4.1)], and a part, $(m_0/m)_{\rm VB}$, arising from the spin polarization of *completely* filled states [see relation (4.3)]. For interstitial 3*d*-TM impurities in silicon it is found—similarly to substitutional ions—that the magnetic-moment part $(m_0/m)_{\rm VB}$ associated with the spin splitting of completely filled states mainly lying in the valence band is very important. For example, in the case of neutral interstitial Fe it is $m_0/m=0.88$, $n(e^{\uparrow})=2$, $n(e^{\downarrow})=0$, $S=1$, and $\alpha^2(e^{\uparrow})=0.51$ (see Fig. 19 and Table III), and according to relations (4.1)–(4.3), it follows that $(m_0/m)_B=0.51$ and $(m_0/m)_{\rm VB}=0.37$. Therefore only 58% of the local magnetization of $Fe^0_{\rm int}$ originates from the partially filled doublet state e. Analysis of ENDOR investigations of interstitial Fe^0 (Refs. 38 and 39), Ti^+, and Cr^+ (Ref. 40) are in good agreement with our calculated values of m_0/m in Table IV.

(b) Charge states, ground-state symmetries, and spin multiplicities. All calculated possible charge (ion) states of interstitial 3*d* impurities in silicon in the ground state are summarized in Table IV. For each charge state the electronic configuration and occupations of the defect-induced states t_2 and e yielding the lowest total energy is given, and the corresponding many-electron ground state is characterized by its spin multiplicity ($2S+1$) and the orbital symmetry Γ in the tetrahedral point group. Contrary to the generally accepted model of Ludwig and Woodbury, we predict *low-spin* ground states for the interstitial 3*d* ions Ti^0, V^+, Ti^-, V^0, and V^-. Available EPR data of interstitial 3*d* ions in silicon (underlined in Table IV) are in agreement with our calculated ground-state configurations, with the following exception: Not including lattice distortions, Cr^0 and Cr^+ are found to have low-spin ground states. For these ions the magnetization of low- and high-spin ground states is significantly different—the total electron spin S differs by $\Delta S=2$—and, therefore, we believe that for the high-spin ground state a spin-induced geometric relaxation might be important (*magnetic pressure* effect[32]).

In comparison to the substitutional site, the charge ratio n_0/Z between the electronic charge n_0 and the nuclear charge Z in the impurity sphere is found to be larger. Moving through the series of neutral interstitials, the ratio n_0/Z is increasing from 0.86 for Ti^0 to 0.99 for Cu^0 (see Table IV). Thus, for Cu^0, local charge neutrality is nearly perfect. Considering different charge states of an interstitial 3*d* impurity, the change in the ratio n_0/Z is only 1% or less and, therefore, the local charge $Q=Z-n_0$ is nearly independent of the charge state. The reason is that the effect of adding or subtracting an electron to or from an interstitial 3*d* point defect is nearly compensated for by charge rearrangements in the valence band.

(c) Single-particle energies and donor and acceptor levels. The calculated energies of the single-particle states associated with neutral interstitial 3*d*-TM impurities in the ground state are shown in Fig. 19. The atomic 3*d* orbital is split into a doublet e branch (dashed curve in Fig. 19) and a triplet t_2 branch (solid curve in Fig. 19) both consisting of spin-up (↑) and spin-down (↓) states. As demonstrated in Fig. 13, the atomic 4*s* orbital is pushed up as an empty resonance state into the conduction band and therefore not shown in Fig. 19. The assumptions in the LW model (see Sec. II A) that an interstitial 3*d* impurity with n valence electrons in silicon exists in a d^n configuration, i.e., the electrons in the atomic 4*s* orbital

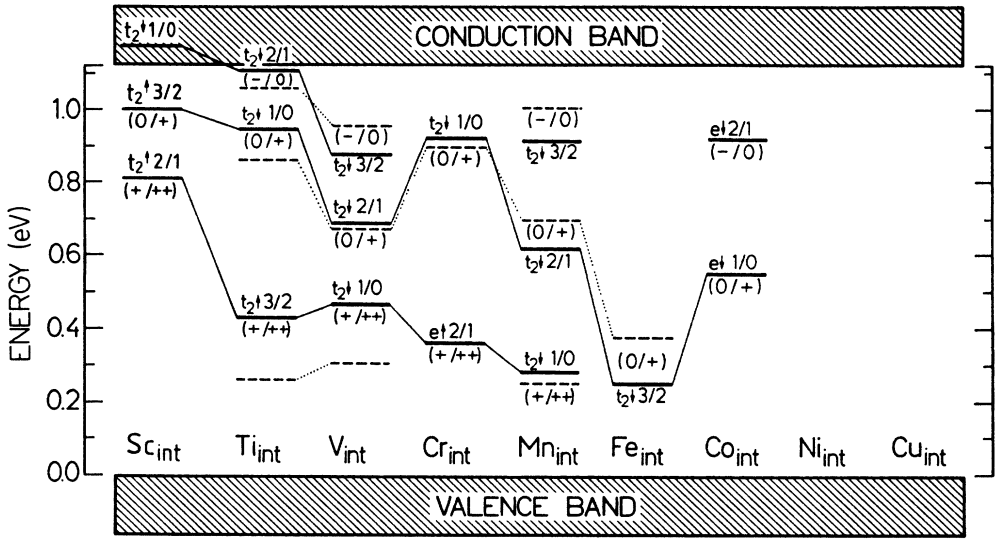

FIG. 20. Calculated (solid lines) and experimental (dashed lines) acceptor and donor levels for interstitial $3d$ impurities in silicon. For each level the related single-particle state (see Fig. 19) and its occupation before and after the ionization is indicated. In the cases of Cr^0 and Cr^+, high-spin states were used.

being promoted to the $3d$ shell, and that the triplet t_2 is energetically below the doublet e, are confirmed by our spin-unrestricted results (Fig. 19), which can be understood qualitatively by the schematic description in Figs. 13 and 15 applied to spin-up and spin-down states. Furthermore, the decreasing crystal-field splitting $\Delta(t_2,e)$ between the e and t_2 branches with increasing atomic number from $\Delta(t_2,e)=1.5$ eV for Ti^0 to $\Delta(t_2,e)=0.4$ eV for Ni^0 can be explained qualitatively by the simple physical picture in Fig. 15: Moving from Ti^0 towards Ni^0, the atomic $3d$ energy decreases and, as a consequence, the interaction between the atomic $3d$ orbital and the t_2 crystal states in the lower conduction-band region (which are mainly responsible for the interstitial impurity level order t_2 *below* e) is being reduced. However, if we consider the occupation numbers of the defect-induced states t_2 and e or the total electron spin S, we find the following: Moving backwards through the interstitial $3d$ series from Ni^0 to Ti^0, the increase in the total electron spin S in steps of $\frac{1}{2}$ between Ni^0 and Cr^0 is interrupted by a jump from $S=2$ for Cr^0 to $S=\frac{1}{2}$ for V^0. This characteristic jump in the total-electron-spin trend, which is reflected by the jump in the otherwise monotonous increase of the single-particle $t_2^{\downarrow}$ energy, is caused by a switch from *high-spin* to *low-spin* ground states between Cr and V. The reason is that, going backwards through the $3d$ series, the splitting between the e and t_2 branches is increasing, and in the case of V and Ti it dominates over the spin spliting. Thus, for interstitial $3d$ impurities to the left of Cr, our theory predicts a *breakdown* of the LW model.

The transition energies between different charge states (Table IV), i.e., the donor and acceptor levels of interstitial $3d$ impurities in silicon obtained by our theory, are shown in Fig. 20 (solid lines) in comparison with established experimental data (dashed lines). For each calculated level position, the related single-particle state and its occupation number before and after the impurity ionization is noted. For example, in the case of interstitial Fe the single-donor energy $(0/+)$ originates from a transition process in which one electron of the $t_2^{\downarrow}$ state is promoted to the conduction band. Therefore, the single-donor level $(0/+)$ of interstitial Fe is related to the single-particle state $t_2^{\downarrow}$ with the occupation-number change 3/2 (denoted as $t_2^{\downarrow}3/2$ in Fig. 20). According to relation (3.9), the single-donor energy $(0/+)$ of Fe_{int} is given by the energy of the single-particle state $t_2^{\downarrow}$ obtained from a self-consistent "transition-state" calculation for $Fe_{int}^{+0.5}$ in which half an electron was removed from threefold occupied triplet state $t_2^{\downarrow}$. As a consequence of electronic relaxation, the single-donor energy $E(0/+)=E_v+0.25$ eV is found to lie below the single-particle energy of the $t_2^{\downarrow}$ state induced by Fe_{int}^0 (see Fig. 19). Similarly, the $(0/+)$ and $(-/0)$ levels of Ti, the three V levels, the $(0/+)$ level of Cr, and the three Mn levels are all related to the triplet state $t_2^{\downarrow}$, whereas the $(0/+)$ and $(+/2+)$ levels of Sc and the $(+/2+)$ level of Ti are derived from $t_2^{\uparrow}$, and the $(+/2+)$ level of Cr and the two Co levels are assigned to $e^{\uparrow}$ and $e^{\downarrow}$, respectively. Interstitial Ni and Cu are predicted to be electrically inactive, i.e., no levels are found to exist within the gap region.

V. SUMMARY

Spin-unrestricted self-consistent electronic and magnetic Green-function calculations for the whole $3d$ transition-metal series in silicon have been performed. Both defect sites of tetrahedral symmetry were considered. Relaxations of the atomic positions were not included.

Our theory predicts *low-spin* ground states for the *early* interstitial ions Ti^0, V^+, Ti^-, V^0, and for the *late* substitutional ions Fe^0, Co^+, Ni^{2+}, Co^0, Ni^+, Co^-, Ni^0, and Cu^+. This is in conflict with the model of Ludwig and Woodbury, but not with available experimental data. Nevertheless, in the case of substitutional Fe and Co the high-spin configurations are higher in energy by only few 0.1 eV, and thus the neglect of lattice relaxations may be crucial. From Sc to Cu all possible charge states with their spin multiplicities and magnetization densities in the ground-state configuration as well as their donor and acceptor levels have been calculated. The ground-state results agree with all EPR data of 3*d* ions in silicon, except for interstitial Cr. We attribute the lack of agreement for Cr^0 and Cr^+ to the local spin density and the atomic-sphere approximation, to the band-gap correction, and to the neglect of a breathing distortion of the impurity neighbors. The calculated deep donor and acceptor energies for the interstitial 3*d* ions reproduce all experimentally observed transitions. Only the double-donor level for Cr obtained by our theory is not found experimentally, which is consistent with the above-mentioned problem for Cr. The prediction of low-spin ground states for interstitial V and Ti is strongly supported by the good agreement between calculated and experimentally observed level positions.

---

*Present addess: Alcatel STR, Friesenbergstrasse 75, CH-8055 Zürich, Switzerland.

†Present address: Fritz-Haber-Institut der Max-Planck-Gesellschaft, Faradayweg 4-6, D-1000 Berlin 33, Federal Republic of Germany.

[1]G. W. Ludwig and H. H. Woodbury, in *Solid State Physics,* edited by H. Ehrenreich, F. Seitz, and D. Turnbull (Academic, New York, 1962), Vol. 13, p. 223.

[2]K. Graff and H. Piper, in *Semiconductor Silicon 81-5* (Electrochemical Society, Pennington, NJ, 1981), p. 331.

[3]L. C. Kimerling, J. L. Benton, and J. J. Rubin, in *Defects and Radiation Effects in Semiconductors* (Institute of Physics, London, 1981), p. 217.

[4]J. W. Chen and A. G. Milnes, Annu. Rev. Mater. Sci. **10**, 157 (1980); A. G. Milnes, *Deep Impurities in Semiconductors* (Wiley, New York, 1973).

[5]E. R. Weber, Appl. Phys. A **30**, 1 (1983).

[6]U. Kaufmann and J. Schneider, in *Festkörperprobleme (Advances in Solid State Physics),* edited by J. Treusch (Vieweg, Braunschweig, 1979), Vol. XX, p. 87; J. Schneider, in *Defects in Semiconductors II,* edited by S. Mahjan and J. W. Corbett (North-Holland, New York, 1983), p. 225.

[7]W. Shockley and W. T. Read, Phys. Rev. **87**, 835 (1952).

[8]H. J. Queisser, Solid-State Electron **21**, 1495 (1978).

[9]A. Rohatgi, J. R. Davis, R. H. Hopkins, P. Rai-Chaudhury, P. G. McMullin, and J. R. McCormick, Solid State Electron. **23**, 415 (1980); R. H. Hopkins, R. G. Seidensticker, J. R. Davis, P. Rai-Chaudhury, and P. d. Blais, J. Cryst. Growth **42**, 493 (1977).

[10]S. M. Sze, *Physics of Semiconductor Devices* (Wiley, New York, 1969).

[11]D. A. von Wezep and C. A. J. Ammerlaan, J. Electron. Mater. **14**, 863 (1985).

[12]H. Feichtinger and R. Czaputa, Appl. Phys. Lett. **39**, 706 (1981).

[13]H. Feichtinger, J. Waltl, and A. Gschwandtner, Solid State Commun. **27**, 867 (1978).

[14]R. Czaputa, H. Feichtinger, J. Oswald, M. Haider, and H. Sitter, Phys. Rev. Lett. **55**, 758 (1985).

[15]B. G. Cartling, J. Phys. C **8**, 3171, 3183 (1975).

[16]L. A. Hemstreet, Phys. Rev. B **15**, 834 (1977).

[17]G. G. DeLeo, G. D. Watkins, and W. B. Fowler, Phys. Rev. B **23**, 1851 (1981); **25**, 4962 (1982); **25**, 4972 (1982).

[18]A. Zunger and U. Lindefelt, Phys. Rev. B **26**, 5989 (1982), **27**, 1191 (1983).

[19]H. Katayama-Yoshida and A. Zunger, Phys. Rev. Lett. **53**, 1256 (1984); Phys. Rev. B. **31**, 7877 (1985); **31**, 8317 (1985); A. Zunger, in *Solid State Physics,* edited by F. Seitz and D. Turnbull (Academic, New York, 1986), Vol. 39, p. 275.

[20]F. Beeler, O. K. Andersen and M. Scheffler, Phys. Rev. Lett. **55**, 1498 (1985); in *Proceediings of the International Conference on Microscopic Identification of Electronic Defects in Semiconductors,* Mater. Res. Soc. Symp. Proc. Vol. 46, edited by N. M. Johnson, S. G. Bishop, and G. D. Watkins (MRS, Pittsburgh, 1985), p. 129.

[21]K. H. Johnson, in *Advances in Quantum Chemistry* (Academic, New York, 1973), Vol. 7, p. 143.

[22](a) J. C. Slater, *The Selfconsistent Field for Molecules and Solids* (McGraw-Hill New York, 1974); (b) *Quantum Theory of Molecules and Solids* (McGraw-Hill, New York, 1963).

[23]L. A. Hemstreet and J. O. Dimmock, Phys. Rev. B **20**, 1527 (1979).

[24]A. A. Lebedev and B. M. Urunbaev, Sov. Phys.—Semicond. **15**, 350 (1981).

[25]M. Scheffler, in *Festkörperprobleme* (Advances in Solid State Physics), edited by P. Grosse (Vieweg, Braunschweig, 1982), Vol. XXII, p. 115.

[26]R. Car, P. J. Kelly, A. Oshiyama, and S. T. Pantelides, Phys. Rev. Lett. **52**, 1814 (1984).

[27]G. A. Baraff and M. Schlüter, Phys. Rev. B **30**, 3460 (1984).

[28]R. Car, P. J. Kelly, A. Oshiyama, and S. T. Pantelides, Phys. Rev. Lett. **54**, 360 (1985).

[29]F. Beeler, M. Scheffler, O. Jepsen, and O. Gunnarsson, Phys. Rev. Lett. **54**, 2525 (1985).

[30]The spin-unrestricted calculations for 3*d* impurities by H. Katayama-Yoshida and A. Zunger—though restricted to the interstitial site in silicon—were for the first time presented together with ours in Bull. Am. Phys. Soc. **30**, 302 (1985).

[31]O. Gunnarsson, O. Jepsen, and O. K. Andersen, Phys. Rev. B **27**, 7144 (1983).

[32]O. K. Andersen, O. Jepsen, and D. Glötzel, in *Proceedings of the Enrico Fermi International School of Physics, Course LXXXIX,* edited by F. Bassani, F. Fumi, and M. P. Tosi (North-Holland, Amsterdam, 1985); O. K. Andersen and O. Jepsen, Phys. Rev. Lett. **53**, 2571 (1984).

[33]U. von Barth and L. Hedin, J. Phys. C **5**, 1629 (1972).

[34]C. Koenig, J. Phys. F **3**, 1497 (1973); H. Dreysse and R. Riedinger, J. Phys. (Paris) **42**, 437 (1981); R. Zeller, J. Deutz, and P. H. Dederichs, Solid State Commun. **44**, 993 (1982).

[35]C. O. Rodriguez, S. Brand, and M. Jaros, J. Phys. C **13**, L333 (1980).

[36]M. Scheffler, F. Beeler, O. Jepsen, O. Gunnarsson, O. K. Andersen, and G. B. Bachelet, J. Electron. Mater. **14**, 45 (1985).

[37]J. Bernholc, N. O. Lipari, S. T. Pantelides, and M. Scheffler,

Phys. Rev. B **26**, 5706 (1982).
[38]S. Greulich-Weber, J. R. Niklas, E. R. Weber, and J.-M. Spaeth, Phys. Rev. B **30**, 6292 (1984).
[39]D. A. van Wezep, T. Gregorkiewicz, E. G. Sieverts, and C. A. J. Ammerlaan, Phys. Rev. B **34**, 4511 (1986).
[40]E. G. Sieverts, D. A. van Wezep, R. van Kemp, and C. A. J. Ammerlaan, in *Defects in Semiconductors,* Vols. 10–12 of *Materials Science Forum,* edited by H. J. von Bardeleben (Trans Tech, Rockport, MA, 1986), p. 729.